Dear Editor

We have addressed all of the comments provided by the two reviewers. The details can be found in our enclosed responses to the reviewers' comments. A version of the paper with major changes highlighted is also enclosed below.

Thank you for handling the review process of this paper.

Sincerely,

Jun Tao and coauthors

Response to Reviewer #1

We greatly appreciate the reviewer for providing the very detailed comments, which have helped us improve the paper quality significantly. We have addressed all of the comments carefully as detailed below. The original comments are in black and our replies are in blue.

Line 7: I'm concerned about reporting the condensation mode MMAD of 0.21 um. This just reflects the midpoint of the diameter bin. If this is the case, why not just report the midpoint of diameter bins for all the modes? Reporting it like data is meaningless.

We agree with this comment and thus have deleted the MMAD for the condensation mode.

Line 19: How is "fine" defined here?

"Fine particles" are defined here as those with aerodynamic diameter smaller than 2.1 μm because the cutoff size of the instrument is at 2.1 μm.

Line 42: Define "IMPROVE" on first usage.

We have revised the text as follows: "the original and revised empirical formulas from the Interagency Monitoring of Protected Visual Environments (IMPROVE) network".

Line 45: MSE are important parameters not just for the IMPROVE equation, but for any application relating mass to optical properties.

We have revised the text as follows: "MSEs of the chemical species are important parameters not only for building the relationships between chemical species and b_{sp} (Hand and Malm, 2007), but also for relating particle mass to its optical properties (Lin et al., 2015; Titos et al., 2012)".

Line 49: Include "based on an assumed size distribution" after "formula…"

Text added as suggested.

Line 60: Yes, the second IMPROVE algorithm was developed for rural (very clean) areas, so it isn't a surprise that it doesn't perform well in urban areas.

We agree with this comment. However, the majority of the studies in China still used the revised formula in urban environment likely because the original IMPROVE formula evidently underestimated b_{sp}. It is thus needed to further assess the uncertainties in these formulas when applying to urban environments.

Line 69: I think the reference here should be "Malm and Hand, 2007". Also, the efficiencies used in the second IMPROVE algorithm are based on an assumed size distribution and composition.

Reference replaced as suggested.

Line 73: Consider removing "According to Mie theory" because Mie theory doesn't specifically speak to the factors hindering the IMPROVE formulas. Line 75: Also, what about assumed hygroscopic growth curves in the IMPROVE algorithm?

We have deleted the text "According to Mie theory". In this study, we only discussed closure of b_{sp} under dry condition, not wet condition.

Line 81: I think the authors mean "inline" when they say "online" data?

We have replaced "online" with "inline" in all the places.

Line 88: Especially in urban areas.

We have revised the text as follows: "Knowledge gained from the present study will improve the assessments of air-quality and climate impact caused by atmospheric particles, especially in urban areas."

Line 116: It would also help to include the other measurements in Table 1, such as the size distributions and nephelometer measurements.

We have added the relevant instruments information in Table 1.

Line 123: Do the authors mean "blank" instead of "background"?

Revised as suggested.

Line 136: What is the expected size cut of the nephelometer? Are there expected size-resolved losses from the tubing from the inlets that affect the size distribution and nephelometer measurements?

We have added the following text in the revised paper to address this comment: "According to the method described in Kulkarni et al. (2011), particle losses in different sizes from the tube are plotted in Fig. S1. Generally, particle losses in the condensation (0.1-0.4 μm), droplet (0.4-2.1 μm) and coarse modes (2.1-10 μm) were less than 1.3%, 0.3% and 0.1%, respectively, suggesting that the particle losses from the tube were minimal. Ambient relative humidity (RH) and temperature were measured by an automatic meteorological station (Vaisala Company, Helsinki, Finland, model MAWS201) at the SCIES site, and the seasonal average of these two meteorological

parameters were 53-75 % and 15-29 °C, respectively."

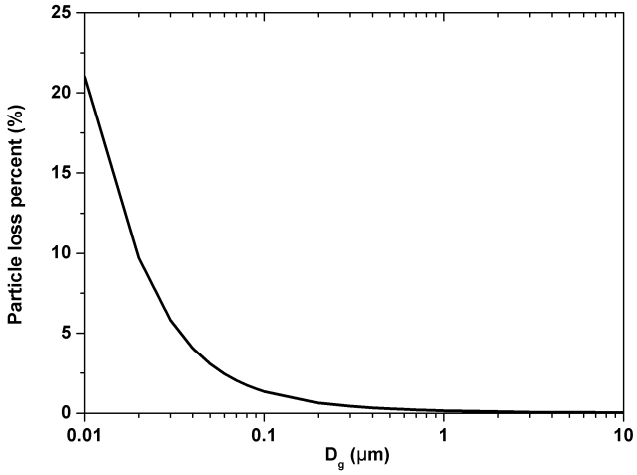

Fig. S1: The estimated particle losses in different size from the tube.

Line 140: Define "RH" at first usage (unless I missed it earlier).

Defined as suggested.

Line 141: Were RH and temperature monitored? What were typical values?

We have added the following text in the revised paper: "Ambient relative humidity (RH) and temperature were measured by an automatic meteorological station (Vaisala Company, Helsinki, Finland, model MAWS201) at the SCIES site, and the seasonal average of these two meteorological parameters were 53-75 % and 15-29 °C, respectively."

Line 179: How were field blanks obtained?

We have added this description in the revised paper: "Moreover, 8 sets of blank samples were also collected for each of the size-segregated particle, $PM_{2.5}$ and PM_{10} samples during the whole sampling period. Two sets of blank filters in each category were put in the samplers without flow for 24 h when seasonal field campaigns finished. The aerosol-loaded filter samples were stored in a freezer at -18 °C before analysis to prevent volatilization of particles."

Line 179: Why was OP so low from the 81mm filters?

Firstly, particle sample showed dot pattern (100-400 dots in every stage) in the size-segregated filters (81 mm filters). Secondly, carbon analyzer only analyzes one punch (0.526 cm^2), which contained 4-5 dots. Thirdly, total carbon loading in fine particle was not high (about 5-30 μg m^{-3}). If its concentration was distributed into 8 stages, then OC

and EC concentrations in each stage would be very low. In addition, OP concentration was much lower than OC and EC. Thus, the uncertainties in OC and EC concentrations would be larger using OP to separate OC and EC in each stage.

Line 201-205: I am not sure of the rationale behind defining the condensation mode as the midpoint diameter of the smallest bin? If the MMAD of the mode is just assigned the midpoint diameter of the bin, what point is there in measuring any size distributions? The MMAD would just be the midpoint diameter of each bin which is meaningless. I don't think you can report the MMAD of the condensation mode if this is how you derive it.

As mentioned above, we have deleted the statement of MMAD for the condensation mode throughout the whole manuscript.

Line 209: I assume this discussion is with respect to the technique by Dong et al. (2004)? It might be helpful to provide more detail here regarding this method, since many of the results depend on it. For example, how were collection efficiencies incorporated into this inversion?

The reviewer is right. Here we indeed refer to the technique of Dong et al. (2004). We have added the key formulas in in section 2.4.

We have also revised the text as follows: "Continuous size-distribution profiles of major chemical species are needed in order to accurately calculate b_{sp} using Mie theory. To improve the resolution of b_{sp}, 401 bins were used for chemical species ranging from 10 nm to 100 μm, with a constant ratio between the adjacent size bins, defined as $\log_{10}(D_{a2}/D_{a1})=0.01$. Further increasing the number of size bins does not have any significant impact on the results, e.g., the changes in b_{sp} are smaller than 1% even if the above ratio of 0.01 is replaced with 0.001. Continuous size-distribution profiles of major chemical species are obtained from the inversion of the measured mass concentration distribution in the size bins of the Anderson 8-stage air samplers, using the technique described in Dong et al. (2004). The key formulas to calculate the normal distribution of density function (f (D, μ, σ)) were summarized as follows:

$$f(D,\mu,\sigma)=\frac{1}{\sqrt{2\pi}\sigma}e^{-\left(\frac{(D-\mu)^2}{2\sigma^2}\right)} \quad (6)$$

$$\mu=\bar{y}-\mu\bar{x} \quad (7)$$

$$\sigma=\frac{n\sum xy-\sum x\times\sum y}{n\sum x^2-(\sum x)^2} \quad (8)$$

Where D is log (D_a), and μ and σ are the mean and standard deviation, respectively, of the log (D_a) in the different modes. x is the inverse function value of the cumulative probability of a standard normal distribution in each bin, y is logarithm of D_a lower limit (e.g. 0.43, 0.65, 1.1, 2.1, 3.3, 4.7, 5.8 and 9.0 μm) in each bin. An example of the calculation process was demonstrated in supplementary.

However, this approach is not applicable for the condensation mode because there is only one size bin in this mode. To obtain the number concentrations of all the concerned chemical species in the condensation mode, MMADs (=10^{μ}) of this mode are calculated according to:

$$MMADs = (D_{a1} \times D_{a2})^{0.5} \quad (9)$$

Where D_{a1} and D_{a2} represent the lower (0.10 μm, limits of detection of Anderson 8-stage air sampler) and upper (0.43 μm) boundaries of this size bin, respectively.

Line 215: Is this size resolved mass from the thermodynamic model on the binned data or the fit data?

We have revised the text as follows: "The ISORROPIA II model was run at the reserved mode (Fountoukis and Nenes, 2007) with input data of K^+, Ca^{2+}, Mg^{2+}, NH_4^+, Na^+, SO_4^{2-}, NO_3^-, Cl^-, RH (40%), and temperature (25°C), to estimate the size-resolved mass concentrations of NaCl, $NaNO_3$, Na_2SO_4, $NaHSO_4$, NH_4Cl, NH_4NO_3, $(NH_4)_2SO_4$, NH_4HSO_4, K_2SO_4, $KHSO_4$, KNO_3, KCl, $MgSO_4$, $Mg(NO_3)_2$, $MgCl_2$, $CaSO_4$, $Ca(NO_3)_2$, $CaCl_2$ and H_2O. Several of these chemical species had extremely low mass concentrations and were thus excluded from the calculation of b_{sp}. Generally, only NaCl, $NaNO_3$, Na_2SO_4, NH_4NO_3, $(NH_4)_2SO_4$, K_2SO_4, $Ca(NO_3)_2$, $CaSO_4$ and H_2O were used to estimate b_{sp} in this study."

Line 217: A section on the DMA and APS size distribution analysis is needed. How was the APS calibrated? How was aerodynamic diameter converted to mobility diameter (or vice versa)? What is the response of the APS to particles of different density? How was density calculated?

The measured particle number concentrations by SMPS and APS were used to assess the accuracy of the estimated particle number concentrations of chemical species in section 3.2.2. We have added the calibration procedure of APS in section 2.2 as follows: "APS was calibrated using 5 sizes solid spheres (polystyrene latex monodisperse)."

We have added the convert formula in section 2.4: "The measured particle number concentrations using SMPS in D_p (similar to D_g) were converted to the particle number concentrations in aerodynamic diameter according to:

$$D_a = D_p/(\rho)^{0.5} \quad (6)$$

$$\rho = \frac{\sum_{chemical\ species} m_i}{\sum_{chemical\ species} \frac{m_i}{\rho_i}} \quad (7)$$

Where, ρ represents the daily average densities of particle, m_i is chemical species mass concentration in a bin, ρ_i is chemical species density. The seasonal average densities of particle were calculated in Fig. S4."

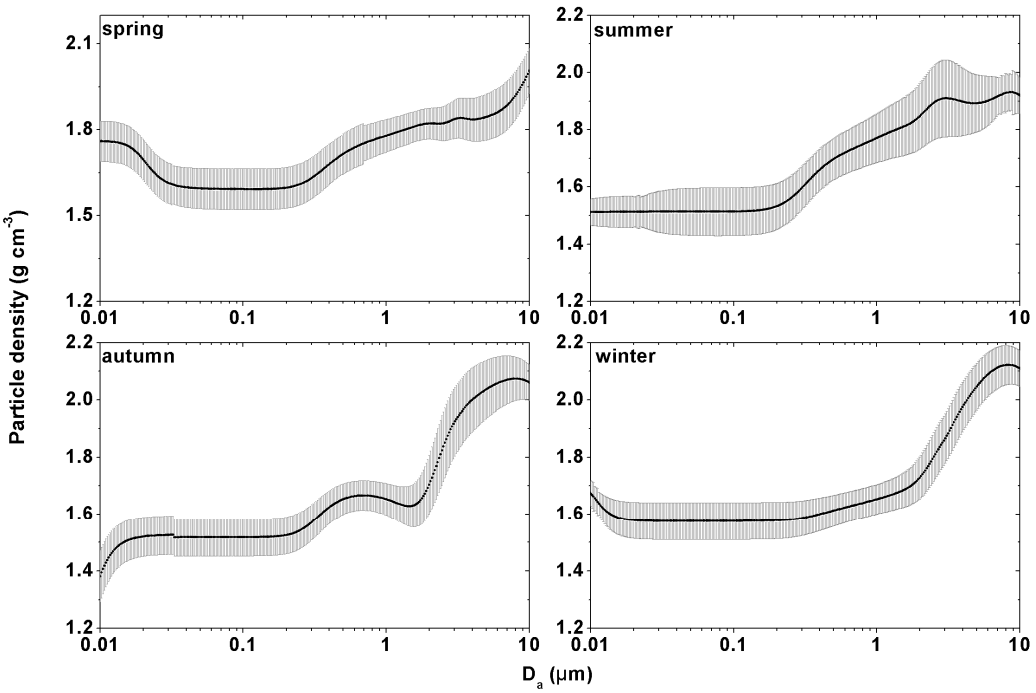

Fig. S4: Continuous log-normal size distributions of seasonal average densities in four seasons.

Line 225: Is PM_{10} here the bulk gravimetric PM_{10} or the summed data from the impactor? Does this include water at the RH of the PM_{10} gravimetric measurement? Particle bound water can still exist for 40% RH.

Here, PM_{10} mass was the sum of the size-segregated mass concentrations. We revised the text as follows: "On annual average, 10±2%, 48±7% and 42±8% of total mass in the size-segregated samples were in the condensation, droplet and coarse modes, respectively, with the average MMADs being 0.78±0.07 μm in the droplet mode and 4.57±0.42 μm in the coarse mode." Yes, particles content a small amount of water even at RH=40% according to the ISORROPIA II model (as shown in Fig.2).

Line 226-227: Units for MMAD?

Units added for MMAD in the revised paper.

Line 226: How were MMADs calculated for the 'continuous' lognormal data?

We have added the key formulas for calculating MMADs in section 2.4. The formula in the droplet and coarse modes : MMADs ($=10^{\mu}$). The formula in the condensation mode: MMADs $=(D_{a1}\times D_{a2})^{0.5}$, where, D_{a1} and D_{a2} represent the lower (0.10 μm, limits of detection of Anderson 8-stage air sampler) and upper (0.43 μm) boundaries of this size bin, respectively. Here MMADs in the condensation mode were only used for estimating the continuous lognormal chemical species mass and number concentrations.

Line 226: Again, reporting an MMAD for the condensation mode is meaningless.

We have deleted the statements on the MMADs for the condensation mode in this manuscript. However, the MMADs in the condensation mode were still used to estimate the continuous lognormal chemical species mass and number concentrations.

Line 229: Define PRD.

We have added the text "the Pearl River Delta (PRD) region".

Line 237: Close to what?

We have revised the text as follows: "Seasonal average particle mass concentrations were evidently lower in summer than in the other seasons for the condensation and droplet modes, and were similar during spring, autumn and winter for all the three modes."

Line 289: What about K^+ in the fine mode?

We have added the size distribution of K^+ in Fig. S5.

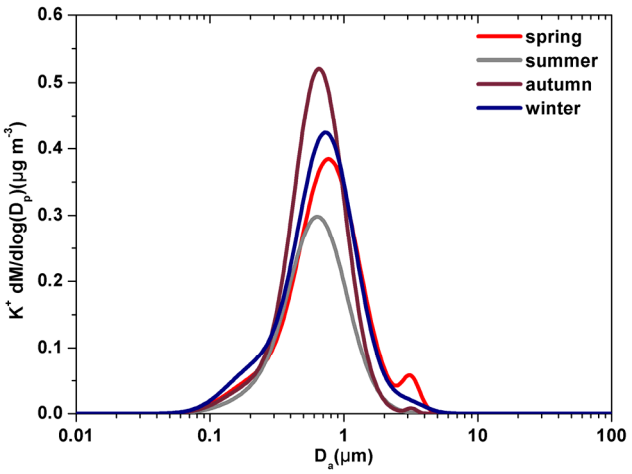

Fig. S5: Continuous log-normal size distributions of K^+ in four seasons.

Line 336: Coarse mode mass fractions also depend on other species. Do the authors mean their absolute concentrations rather than relative concentrations?

Yes, coarse mode mass fraction also depended on chemical species especially OM and crustal element oxides. Here, PM_{10} mass concentration was the absolute (not relative) concentration. We have revised the text as follows: "Annual average PM_{10} concentrations (46 μg m^{-3}) in 2015-2016 in the PRD region were about 40% lower than that (76 μg m^{-3}) in 2006-2007, which further supported the above hypothesis."

Line 339: Change title to "Closure of particle mass, number concentration, and bsp"

Revised as suggested.

Line 345: Was sulfate fully neutralized for the duration of the study?

Sulfate was fully neutralized by NH_4^+, Na^+, K^+ and Ca^{2+} according to the ISORROPIA II model.

Line 355: Was 5% used here?

We used 5.3% as stated in the supplementary. We have added such explanation in the revised paper: "Alternatively, crustal element oxides mass concentration was estimated from Ca^{2+} mass concentration because of their good correlations (slope=0.053, R^2=0.79) as was found in a previous study (Fig. S6) (Tao et al., 2017b). It was suggested that Ca^{2+} accounted for 5.3% of crustal element oxides in $PM_{2.5}$ in urban Guangzhou, a value that is close to the content of Ca^{2+} (5.0%) in soil dust source profiles (representing crustal element oxides) in $PM_{2.5}$ in cities of southern China (Sun et al., 2019). Because $CaSO_4$ and $Ca(NO_3)_2$ were mainly from the reactions between calcium oxide and acids (e.g. H_2SO_4 and HNO_3), the estimated mass concentration of crustal element oxides needs to deduct those of $CaSO_4$ and $Ca(NO_3)_2$."

Line 362: I am not sure what is meant here by the "total"? How was "total" derived in this context?

We have deleted the word "total". We originally referred to the sum of the condensation, droplet and coarse mode mass concentrations.

Line 371: Same comment as the previous.

The word "total" is now deleted.

Line 382: Please provide more details regarding this method.

We have added the formula for calculating number concentration of chemical species in section 2.4, which reads: "$N_{i,j}$ is number concentration of chemical species calculated by the formula (3).

$$N = \frac{6C}{\pi \rho D^3} \quad (3)$$

Where, N is chemical species number concentration, C is chemical species mass concentrations, ρ is density of chemical species (Table S1), D is geometric diameter (D_g) of chemical species.

The particle number concentrations in aerodynamic diameter (D_a) were converted to

the particle number concentrations in D_g (similar to D_p) according to:

$$D_a = D_g/(\rho)^{0.5} \quad (4)$$

$$\rho = \frac{\sum_{chemical\ species} m_i}{\sum_{chemical\ species} \frac{m_i}{\rho_i}} \quad (5)$$

Where, ρ represents the daily average densities of particle, i is chemical species, m_i is chemical species mass concentration in a bin, ρ_i is chemical species density. The seasonal average densities of particle were calculated in Fig. S4."

Line 384: This would be expected because of the diameter-cubed dependence between number and mass.

We agree with this comment and we deleted the irrelevant statement.

Line 386: What is the difference in the definition of the estimated NMAD of the number concentrations of individual species and the NAMD of particle number concentrations? (individual versus particle?). I think an issue here is that the constant 0.21 m value is meaningless.

The sums of the individual species number concentrations were the particle number concentrations. We have revised the text as follows: "The estimated number mean aerodynamic diameters (NMADs) of the number concentrations of individual chemical species mainly distributed in the range of 100-120 nm. The estimated NMADs of particle number concentrations (sum of individual chemical species number concentrations in the same size bin) were close to about 100 nm in the four seasons, which was larger than the NMADs (30-70 nm) of the simultaneously measured particle number concentrations by the SMPS and APS (Fig. 4)."

Line 392: What densities were used?

The densities of the individual chemical species are listed in Table S1.

Table. S1 The refractive indices and densities of chemical species.

Chemical species	refractive index	density(g cm^{-3})	Chemical species	refractive index	density(g cm^{-3})
NaCl	1.54-0i	2.16	$Ca(NO_3)_2$	1.53-0i	2.50
$NaNO_3$	1.59-0i	2.26	H_2O	1.33-0i	1.00
Na_2SO_4	1.48-0i	2.68	OM	1.55-0i	1.40
$(NH_4)_2SO_4$	1.53-0i	1.76	EC	1.80-0.54i	1.50
NH_4NO_3	1.55-0i	1.73	crustal element oxides	1.56-0.01i	2.66
K_2SO_4	1.49-0i	2.66	unidentified fraction	1.58-0.01i	2.00
$CaSO_4$	1.57-0i	2.61			

Line 397: The reasoning here isn't clear. The size segregated chemical mass species concentrations should be dry. Unless the authors mean that particle bound water was associated with a gravimetric measurement, the individual species mass do not include water.

The size segregated particle mass concentrations and chemical species mass concentrations were weighted and estimated under a dry condition (temperature = 25°C and relative humidity = 40%). Besides chemical species, water was also resolved in the size segregated samples according to ISORROPIA II model (Fig. 2). In contrast, the particle number concentrations were measured under dry condition (relative humidity < 30%). Moreover, little water was resolved in the size segregated samples according to ISORROPIA II model. To some extent, chemical species likely internally mixed with chemical species in the real world and resulted in the larger diameter of chemical species than the measured ones under dry condition.

Line 418-420: I am unclear as to why scattering efficiencies are being discussed here?

We agree with this comment and have deleted this part.

Line 421-423: This is the first discussion of these design flaws – are the authors referring to the single bin for the condensation mode?

Yes, it was because we cannot get the MMAD in the condensation mode and cannot accurately estimate the number concentration especially those of <100 nm.

Line 426: How much higher?

We have added this text: "On annual average, the estimated particle number concentrations in the range of 430 nm-10 μm based on the size-segregated chemical species mass concentrations were 33±42% higher than those measured by the SMPS and APS."

Line 429: How do the authors know that EC was internally mixed with OM or inorganic salts during this study?

Here we only tried to interpret the possible reasons of the overestimation of the particle number concentrations by the size-segregated chemical species mass concentrations. We have deleted this statement in the revised paper.

Line 433-434: The reasoning here is unclear. What are the estimation errors and models?

This refers to the estimated particle number concentrations by the size-segregated chemical species mass concentrations using the inversion technique and ISORROPIA II model. We have revised the text as follows: "To some extent, the intercepts represent

the measurement errors of SMPS and APS and estimation errors of the inversion technique and ISORROPIA II models."

Line 448: The authors need to provide more details on how they derived bsp. What refractive indices did they use, how did they calculate them, which number size distributions did they use, etc.

We have added description of several key input parameters of Mie model for estimating b_{sp}, which reads: "Daily b_{sp} was estimated using Mie model (in section 2.4) with input parameters including refractive indices, densities and number concentrations in 401 bins of chemical species (NaCl, $NaNO_3$, Na_2SO_4, $(NH_4)_2SO_4$, NH_4NO_3, K_2SO_4, $CaSO_4$, $Ca(NO_3)_2$, H_2O, OM, EC, crustal element oxides and unidentified fraction). The refractive indices and densities of above chemical species are summarized in Table S1."

Line 455: Why "especially the inversion technique method"?

We agree that this statement is a bit confusing and we have deleted the word "especially".

Line 460: What do the authors mean that OC was underestimated by the OC/EC protocol?

This is because OC of size-segregated samples is defined as OC1 + OC2 + OC3 + OC4 rather than OC1 + OC2 + OC3 + OC4 + OP due to the low OP concentration in each bin.

Line 468, 472: Do the authors mean "inline" data?

We have replaced the word as suggested.

Line 502: What did the authors use for refractive indices for the "unidentified fraction"?

We have added the refractive indices and densities of chemical species in supplementary (Table S1). The refractive index of the unidentified fraction is 1.58-0.01i.

Line 517, 521: I am not sure what is meant by "particle and chemical species". What is the distinction?

Particle MSE was estimated by sum of b_{sp} from individual chemical species divided by sum of particle mass concentration. MSEs of individual chemical species was estimated by b_{sp} using Mie model according to its particle number in 401 bins, refractive index and density divided by its mass concentration. Thus, we have clarified this part as follows: "Here, only the MSEs of $(NH_4)_2SO_4$, NH_4NO_3, OM, EC, crustal element oxides and unidentified fraction in the condensation, droplet, fine (sum of condensation

and droplet), and coarse modes were estimated (Table 3), considering these chemical species accounted for more than 90% of the estimated b_{sp}. However, particle MSEs in the condensation, droplet, fine and coarse modes were estimated by sum of b_{sp} from individual chemical species divided by sum of particle mass"

Line 540: This points back to the previous comments as well. Was "particle MSE" estimated by summed bsp from individual species divided by summed particle mass, or was bsp calculated for "particle", which then would require a "particle" refractive index? It would help if the authors provided details for how these things are calculated (see comment for line 448).

See our clarification in the previous comment.

Line 577: Define MMGD

We have redefined the GMMD as geometric mass mean diameters (MMGD) of chemical species ($(NH_4)_2SO_4$, NH_4NO_3 and OM), which was converted from MMAD and its density according to the formula (6) in section 2.4.

Line 626-627: Sentence is unclear.

We have simplified this part as follows: "Different from the approach used for fine particle MSE, the MSEs of $(NH_4)_2SO_4$, NH_4NO_3 and OM in the droplet mode were determined using measurement-based their mass size distributions prescribed as log-normal size distributions. MSEs of these chemical species strongly depend on their size-distributions, which were defined here as log-normal distributions with three parameters including mass concentration (in the range of 0.43 - 2.1 μm), MMAD and standard deviation (σ)."

Line 630: How were sigma values calculated?

We have added the key formulas in section 2.4, which included the calculation method of sigma and MMAD.

Line 653: What does "bulk particle" mean?

The bulk particle means the sum mass concentration of the condensation, droplet and coarse modes. We have revised the text as follows: "and particle mass, NO_3^-, OC, Na^+, Ca^{2+} and Cl^- in both droplet and coarse modes."

Line 670: Sea salt in the IMPROVE formula is assumed to have a mass mean diameter of 2.5 um, so it is assumed to be in the coarse mode with the tail extending into the PM2.5 mode. Figures and Tables: Table 2: Define size range of condensation, droplet and coarse modes. Again, reporting 0.21 um for all condensation mode MMAD is

meaningless. Define “MMAD” in the caption.

We agree with this comment, and we also suspected that sea salt may distribute in the tail of $PM_{2.5}$. However, we cannot find NaCl in $PM_{2.5}$ according to the ISORROPIA II model. In fact, we found a large amount of Na_2SO_4 in $PM_{2.5}$, which would be related with aged sea salt. Here, we referred sea salt as NaCl rather than Na_2SO_4. We have deleted 0.21 μm for all condensation modes in Table 2. We defined the size ranges in the different modes in Table 2 and defined MMAD in the subtitle.

Table 3: Define size range of condensation and droplet modes. Again, reporting 0.21 um for all condensation mode MMAD is meaningless. Define “MSE” and “MMAD” in the caption. Include wavelength and relative humidity (Dry = ?%) in the caption or subtitle.

We have deleted 0.21 μm for all the condensation modes in Table 3. We have added the size ranges for the different modes in Table 3. Table caption revised as suggested.

Figure 1: Define “PRD” in the caption.

Revised as suggested.

Figure 2: Was CaSO4 and Ca(NO3)2 subtracted out of the soil formula when using Ca to calculate soil? These figures suggest that EC mass size distributions are larger than OM distributions? Are these stacked? If so EC » SO4 but mass concentrations in Table 2 suggests this is not the case. The presentation is somewhat confusing. Keep the y-axis the same for all seasons for easier comparisons.

We have clarified the relationships between the estimated soil mass concentration and calcium salts ($CaSO_4$ and $Ca(NO_3)_2$) in section 3.2.1, which reads: “Alternatively, crustal element oxides mass concentration was estimated from Ca^{2+} mass concentration because of their good correlations (slope=0.053, R^2=0.79) as was found in a previous study (Fig. S6) (Tao et al., 2017b). It was suggested that Ca^{2+} accounted for 5.3% of crustal element oxides in $PM_{2.5}$ in urban Guangzhou, a value that is close to the content of Ca^{2+} (5.0%) in soil dust source profiles (representing crustal element oxides) in $PM_{2.5}$ in cities of southern China (Sun et al., 2019). Because $CaSO_4$ and $Ca(NO_3)_2$ were mainly from the reactions between calcium oxide and acids (e.g. H_2SO_4 and HNO_3), the estimated mass concentration of crustal element oxides needs to deduct those of $CaSO_4$ and $Ca(NO_3)_2$.”

The mass size distributions of OM were in fact larger than those of EC in four seasons, although Figure 2 seems to show an opposite result, which was due to the overlap of chemical species. The annual average size distributions of the individual species of $(NH_4)_2SO_4$ OM and EC are plotted below. We have also revised the scale of the y-axis in all the figures.

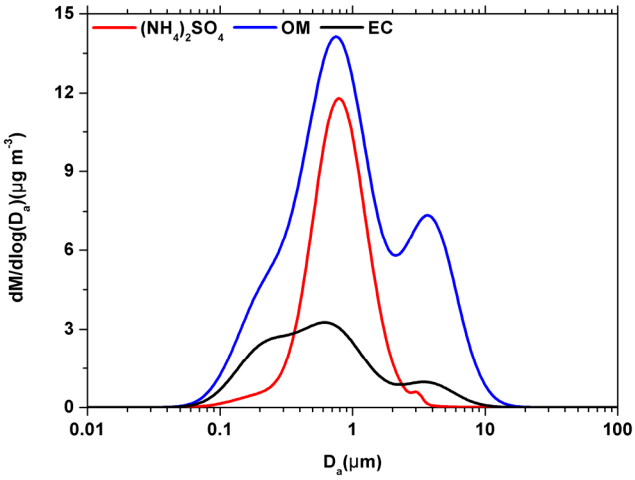

Fig. Suppl. Continuous log-normal size distributions of $(NH_4)_2SO_4$, OM and EC.

Figure 3: Similar comments as previous caption.

See our response in the previous comment.

Figure 4: It would help to plot the APS data in terms of mass or volume instead of number based on the size range- the larger modes would be more visible.

Although it may be more visible using mass or volume data than using number data, it is the number concentration that was directly measured by SMPS and APS. Moreover, the input data of Mie model also need number concentration of chemical species. Thus, we used the measured number concentrations by SMPS and APS to close the estimated number concentrations of chemical species.

Figure 6: Include wavelength, relative humidity conditions, and size range. Is this total bsp?

We revised the caption as follows: "Fig. 6. Correlations between the measured b_{sp} in TSP at wavelength of 520 nm under dry condition (relative humidity <30%) and estimated b_{sp} in PM_{10} at wavelength of 550 nm under dry condition (relative humidity =40%) in four seasons."

Figure 7: Similar comments to figure 2. I don't understand how the mass of sulfate can be so much higher than EC yet the EC scattering is greater?

Figure 7 shows the contributions of chemical species including NaCl, $NaNO_3$, Na_2SO_4, NH_4NO_3, $(NH_4)_2SO_4$, K_2SO_4, $CaSO_4$, $Ca(NO_3)_2$, H_2O, OM, EC, crustal element oxides and unidentified fraction to the estimated b_{sp} in the different sizes (0.1-10μm in 401 bins). The different size distributions between $(NH_4)_2SO_4$ and EC caused the higher contribution from $(NH_4)_2SO_4$ to the estimated b_{sp} despite its lower mass concentrations.

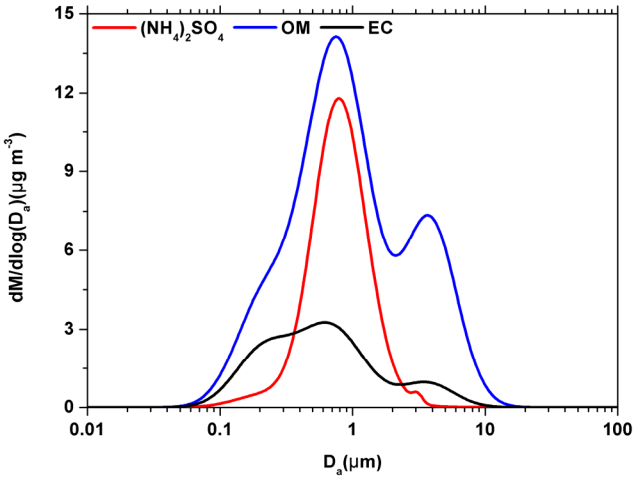

Fig. Suppl. Continuous log-normal size distributions of $(NH_4)_2SO_4$, OM and EC.

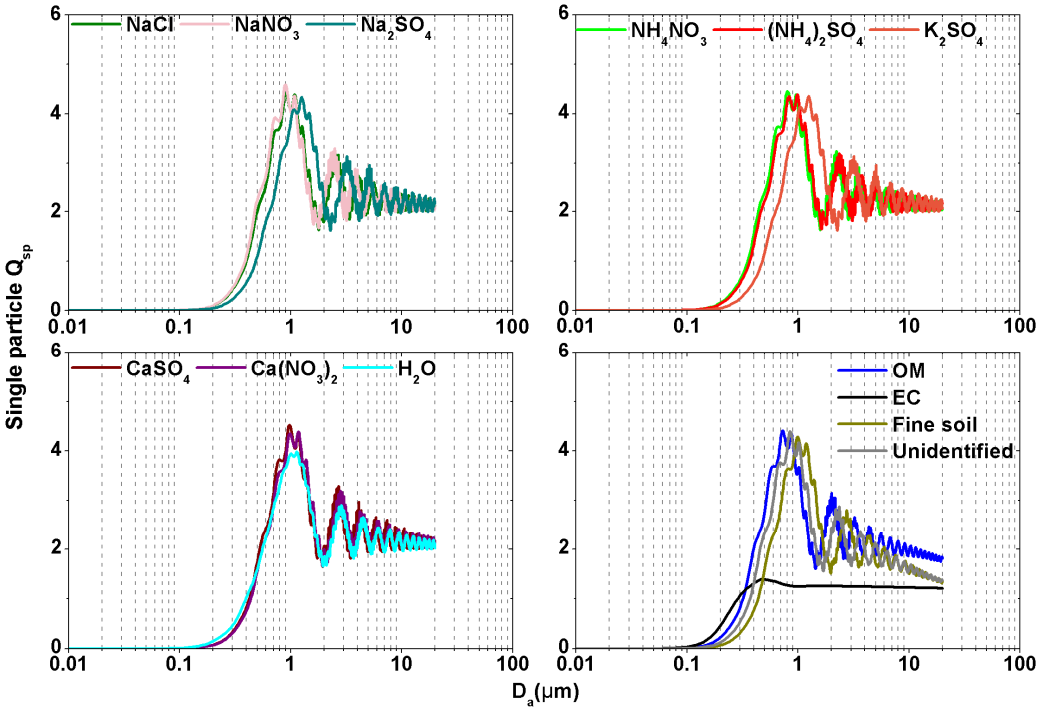

Fig. S3: Single particle scattering efficiencies of the dominant chemical species.

Figure 8: Define "MSE", "fine", wavelength, and relative humidity conditions in the caption.

Figure caption has been revised as suggested.

Figure 9: Caption doesn't include any information on MSE. Also include wavelength, and relative humidity conditions in the caption.

Figure caption has been revised as suggested.

Response to Reviewer #2

We greatly appreciate the reviewer for providing the detailed comments, which have helped us improve the paper quality significantly. We have addressed all of the comments carefully as detailed below. The original comments are in black and our replies are in blue.

One thing that I recommend doing is to calculate your MSEs also by using multiple linear regression (MLR). Now you calculated them with a Mie model. That is fine and scientifically justified but it also has its uncertainties, for instance related to refractive indices etc. Your data is good for MLR and that would give another estimate for the MSEs. MLR is quick and easy to do – even with Excel – and that is also actually inversely the way air quality data would be used for estimating visibility from PM2.5 filter data. Doing that you would have an additional uncertainty estimate and a closure of MSEs.

We agree with the reviewer that it is worth and relatively easy to use the multiple linear regression (MLR) model to estimate MSEs, as we have done in several of our previous studies (Tao et al., 2014a, 2014b, 2015, 2016). In fact, we have recently completed another study comparing MSEs calculated from using various methods including the MLR model. We chose not to present the results here from this particularly method because (1) the paper is already very long, (2) the focus of the present study is to investigate the causes of the variations in the estimated MSEs (not the absolute errors in using the Mie model), and (3) a systematic study on model differences in the calculated MSEs will be presented in a separate study.

Having done that I suggest you make an additional scatter plot and linear regressions of scattering coefficient calculated with the Mie-derived MSEs, with the MLR-derived MSEs and with IMPROVE MSEs vs. measured scattering coefficient. Now you have written in the text new MSEs and written how they differ from the IMPROVE MSEs but the full comparison for the Guangzhou air is missing, that would be the linear regressions I suggested. How well do the different MSEs predict the observed scattering?

As explained in the previous comment, we chose not to present the MLR-derived MSEs in this study. Here, we focused on comparing the differences in the estimated b_{sp} using the estimated MSEs of chemical species and the measured b_{sp} in section 3.3.1. We have revised the explanation as follows: "Generally, good correlations (R^2> 0.79) were found between the measured and estimated b_{sp} using the average MSEs of chemical species in Table 3 with the slopes being 0.85, 0.84, 0.76 and 0.84 in spring, summer, autumn and winter, respectively (Fig. S8). Thus, the estimated MSEs of chemical species in Table 3 were underestimated."

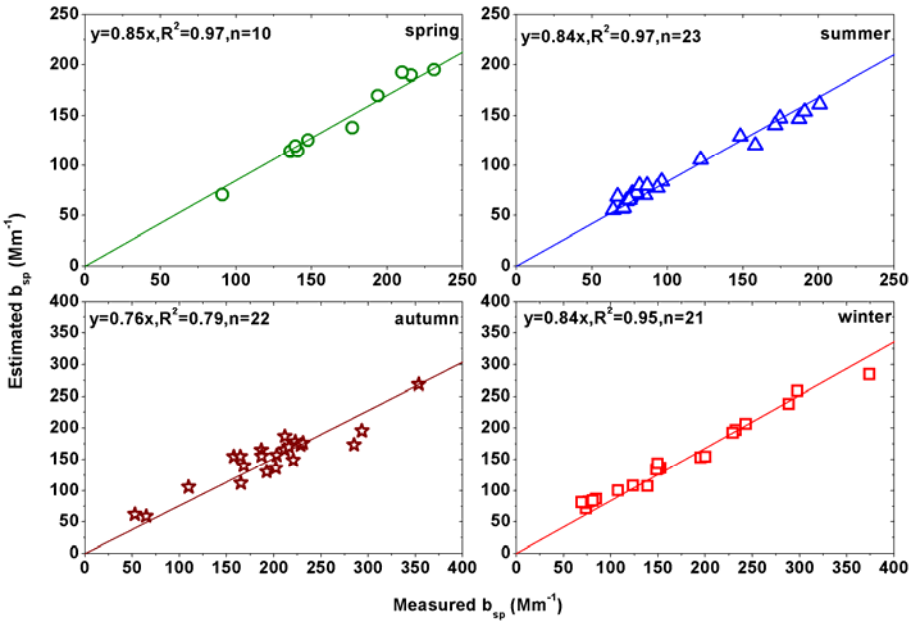

Fig. S8: Correlations between the measured b_{sp} (<100 μm) at wavelength of 520 nm under dry condition (relative humidity <30%) and estimated b_{sp} (<10 μm) using average MSEs of chemical species at wavelength of 550 nm under dry condition (relative humidity =40%) in four seasons.

The estimated b_{sp} depended on both the mass concentrations and MSEs of chemical species. Thus, it is difficult to assess the difference in the estimated b_{sp} only using the MSEs chemical species. In fact, there are large uncertainties from mass concentrations. As mention above, we have recently finished another study to address this issue, which tentatively titled "The differences in the estimated particle scattering coefficient using the different methods in urban Guangzhou of South China".

As Fig 1 and 2 show, on annual average, the estimated mass concentrations of $(NH_4)_2SO_4$ and NH_4NO_3 in $PM_{2.5}$ using the ISORROPIA II model were 42±24% and 33±44%, respectively, lower than those using the original IMPROVE formula. However, the estimated MSEs of the $(NH_4)_2SO_4$, NH_4NO_3 and OM in the fine mode using the multiple models were 47%, 50% and 15%, respectively, higher than those in the original IMPROVE formula. As a result, the differences in annual average contributions of the dominant chemical species were less than 3% between using the multiple models and the original IMPROVE formula. In contrast, the estimated mass concentrations of $(NH_4)_2SO_4$, NH_4NO_3 and organic matter (OM) using the multiple models were 93±16%, 96±9% and 60±32%, respectively, lower in the small mode and 20±50%, 674±569% and 43±68%, respectively, lower in the large mode than those from using the revised IMPROVE formula. The differences in the estimated MSEs of $(NH_4)_2SO_4$, NH_4NO_3 and OM were less than 13% between using the multiple models and the revised IMPROVE formula. Generally, the estimated contributions of the dominant chemical species ($(NH_4)_2SO_4$, NH_4NO_3 and OM) to the measured b_{sp} under

dry condition using the original and revised IMPROVE formula were acceptable.

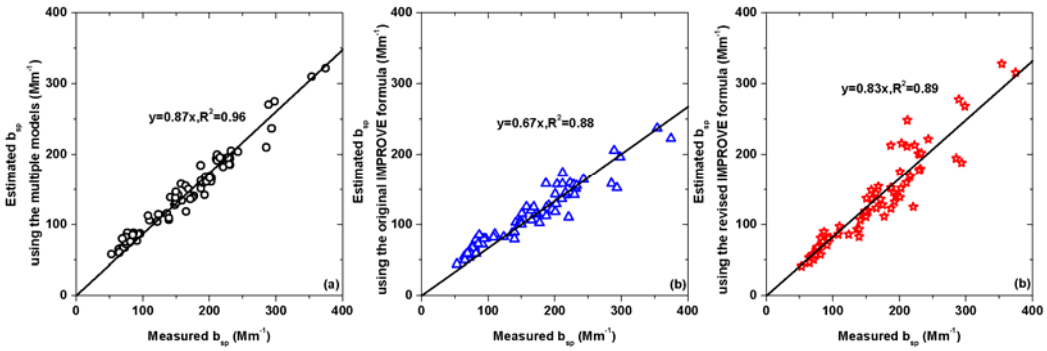

Fig. Suppl.1. Correlations between the measured b_{sp} and the estimated b_{sp} using the multiple models (a), the original IMPROVE formula (b) and the revised IMPROVE formula (c).

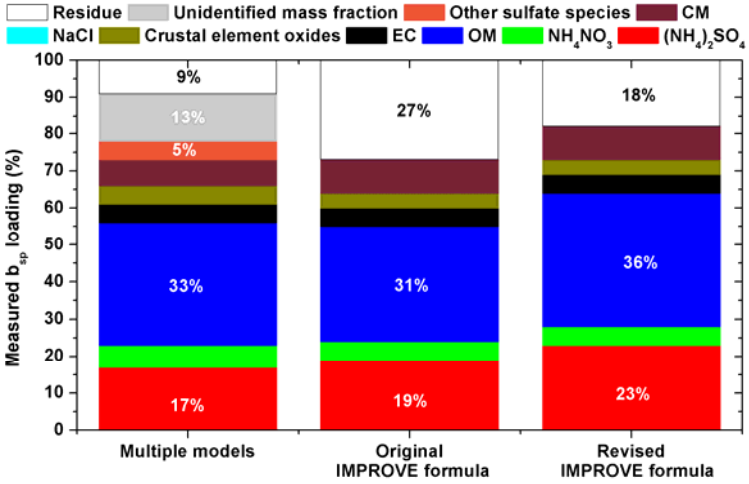

Fig. Suppl.2. Contributions of chemical species to the measured b_{sp} using the multiple models, the original IMPROVE formula and the revised IMPROVE formula.

Another thing I miss is equations. For example equations of how you calculated MSE, the mean diameters you are using and also chemistry: Did you dry the sampling air for the impactor? If not the particles are larger and get collected on the upper stages which affects the inverted size distributions and ultimately the Mie-modeled scattering. At least some discussion of this would be good.

We have added key formulas in section 2.4. We have revised the text as follows: "Particle MSE was estimated by the sum of b_{sp} from individual chemical species divided by sum of particle mass concentration according to:

$$\mathrm{MSE} = \frac{\int_0^{D_{i,j}^{max}} b_{sp}\ dD_{i,j}}{\int_0^{D_{i,j}^{max}} C\ dD_{i,j}} \quad (1)$$

Where i is chemical species, j is chemical species size, $D_{i,j}$ is the chemical species diameter, and C is chemical species mass concentration."

Yes, the size segregated samples were collected under the ambient condition rather than the dry condition. We believe the MMADs of chemical species under the ambient would be larger than those under the dry condition due to the particle hygroscopic properties. However, we cannot quantify the difference in the size distribution under the ambient and dry conditions. We highlighted this factor in the analysis of closure between the measured and estimated b_{sp} in section 3.2.3. We have revised the discuss as follows: "Moreover, the size distributions would be different under dry and ambient conditions due to the particle hygroscopic properties. In fact, the NMADs of particle measured by SMPS and APS under dry condition were less than those measured by the size-segregated sampler under ambient condition according to section 3.2.2. Thus, the estimated b_{sp} based on size distributions of chemical species would be systematically higher to some extent than the measured b_{sp} under dry condition."

Detailed comments
L131 " ... geometric diameter (Dg) ..." The widely used meaning of Dg is the geometric mean diameter of a particle number size distribution. So use Dp. for the aerodynamic diameter use Da.

We have revised the descriptions as follows: "Particle number concentration for particles in the range of 14 nm - 615 nm in mobility diameter (D_p) was measured….."

L137-138. Nephelometer: did you calibrate it?

We have added the statement: "Zero calibration was performed every day with zero air, and span check was done every 3 days using HFC-R134a gas."

L197: explain the Mie model in a bit more detail.

We have added the following description in section 2.4:

b_{sp} was estimated by the Mie model as follows:

$$b_{sp} = \int_0^{D_{i,j}^{max}} \frac{\pi}{4} D_{i,j}^2 Q_{sp}(m_{i,j}, D_{i,j}, \lambda) N_{i,j} dD_{ij} \quad (2)$$

Where Q_{sp} is single-particle scattering efficiency of chemical species (Fig. S3), $m_{i,j}$ is refractive index of chemical species (Table S1), λ is 550 nm, and $N_{i,j}$ is number concentration of chemical species calculated by the formula (3).

$$N = \frac{6C}{\pi \rho D^3} \quad (3)$$

Where N is chemical species number concentration, C is chemical species mass concentrations, ρ is density of chemical species (Table S1), and D is geometric diameter (D_g) of chemical species.

The particle number concentration in aerodynamic diameter (D_a) was converted to the particle number concentration in D_g (similar to D_p) according to:

$$D_a = D_g/(\rho)^{0.5} \quad (4)$$

$$\rho = \frac{\sum_{chemical\ species} m_i}{\sum_{chemical\ species} \frac{m_i}{\rho_i}} \quad (5)$$

Where ρ represents the daily average density of particle, i is chemical species, m_i is chemical species mass concentration in a bin, and ρ_i is chemical species density. The seasonal average densities of particle are shown in Fig. S4.

L201, define MMAD and give the formula L206 "limit of detection" is wrong here, that expression is related to concentration measurements

We have given the formula for calculating MMAD in section 2.4. We believe MMAD was related with the mass concentrations in each bin of size-segregated sampler. However, only one bin is designed in the condensation mode, and we thus used formula (9) to estimate MMAD in the condensation mode.

L248 "As expected" – why would you expect this?

It was because SO_4^{2-}, NO_3^- and NH_4^+ are mainly formed through aqueous-phase reactions in moisture conditions in the PRD region. Thus, most of them should be distributed in the droplet mode.

L266 "NO3 mainly exists in the form of ammonium nitrate..." you have data on the inorganic ion concentrations but how did you calculate concentration of ammonium sulfate and ammonium nitrate? Give a couple of formulas.

The chemical species including NH_4NO_3, $(NH_4)_2SO_4$ were estimated by the ISORROPIA II model, which was run at the reserved mode with input data of K^+, Ca^{2+}, Mg^{2+}, NH_4^+, Na^+, SO_4^{2-}, NO_3^-, Cl^-, RH (40%), and temperature (25°C). The ISORROPIA II model has an open source code. The key formulas were described in Fountoukis and Nenes (2007).

L385 "NMAD" – give formula

The NMAD is the number mean aerodynamic diameter, which is calculated the same way as the MMAD (mass mean aerodynamic diameter) except of substituting the mass concentration with number concentration. The actual formula for NMAD calculation can be expressed as:

$$\mathrm{NMAD} = \frac{\int_0^{D_i^{max}} \frac{6C}{\pi\rho {D_i}^2}}{\int_0^{D_i^{max}} \frac{6C}{\pi\rho {D_i}^3}}$$

L574 "mass median geometric diameter (MMGD)" I have never heard of. Define. Consider using some other descriptive diameter that has been presented in literature.

The mass median geometric diameter derived from mass median aerodynamic diameter. The definition of the geometric mass mean (or median) diameters and mass mean (or median) aerodynamic diameters can be found in Hand and Malm (2007). Thus, we revised mass median geometric diameter (MMGD) as geometric mass mean diameters (GMMD).

Hand, J. L., and Malm, W. C.: Review of the IMPROVE equation for estimating ambient light extinction coefficients, CIRA, Colorado State University, 2007.

Fig. 4. Are the diameters of the SMPS data and the APS data both aerodynamic or what? The gap is huge, try to explain it.

The diameter of the SMPS data is D_p, while the diameter of the APS data is D_a. the gap of number concentrations between using SMPS and using APS were mainly due to the different dlog(D). The dlog(D_p) and dlog(D_a) were 0.015 and 0.031, which meant the measured number concentration by SMPS would be higher by 2 times (0.031/0.015) than those measured by APS at the same size.

Fig 5. The numbers in the x and y axes cannot be true. In Guangzhou number concentrations are in the range of thousands, now the max concentration is about 400 /cc.

Total particle number concentration in the range of 10 nm-10 μm measured by the SMPS and APS were 7038±2250 cm^{-3}, 9774±1471 cm^{-3}, 5694±1942 cm^{-3} and 10801±2986 cm^{-3}, respectively, in spring, summer, autumn and winter. As shown in Fig. 4, most of particles distributed in the condensation mode (<430 nm). Here, Fig. 5 shows the correlations between the estimated and SMPS- and APS-measured particle number concentrations (430 nm-10 μm) in four seasons. To avoid misunderstanding, we revised the figure caption as follows: “Fig. 5. Correlations between the estimated and SMPS- and APS-measured particle number concentrations in the size range of 430 nm-10 μm in four seasons.”

Impact of particle number and mass size distributions of major chemical components on particle mass scattering efficiency in urban Guangzhou of South China

Jun Tao[1,*], Zhisheng Zhang[1], Yunfei Wu[2], Leiming Zhang[3,*], Zhijun Wu[4], Peng Cheng[5], Mei Li[5], Laiguo Chen[1], Renjian Zhang[2], Junji Cao[6]

[1]South China Institute of Environmental Sciences, Ministry of Environmental Protection, Guangzhou, China

[2]RCE-TEA, Institute of Atmospheric Physics, Chinese Academy of Sciences, Beijing, China

[3]Air Quality Research Division, Science and Technology Branch, Environment and Climate Change Canada, Toronto, Canada

[4]State Key Joint Laboratory of Environmental Simulation and Pollution Control, College of Environmental Sciences and Engineering, Peking University, Beijing, China

[5]Institute of Mass Spectrometer and Atmospheric Environment, Jinan University, Guangzhou, China

[6]Key Laboratory of Aerosol Chemistry and Physics, Institute of Earth Environment, Chinese Academy of Sciences, Xi'an, China

*Correspondence to: (Leiming Zhang) leiming.zhang@canada.ca or (Jun Tao) taojun@scies.org

Abstract. To grasp the key factors affecting particle mass scattering efficiency (MSE), particle mass and number size distribution, $PM_{2.5}$ and PM_{10} and their major chemical compositions, and particle scattering coefficient (b_{sp}) under dry condition were measured at an urban site in Guangzhou, south China during 2015-2016. On annual average, 10±2%, 48±7% and 42±8% of PM_{10} mass were in the condensation, droplet and coarse modes, respectively, with mass mean aerodynamic diameters (MMADs) of 0.78±0.07 in the droplet mode and 4.57±0.42 μm in the coarse mode. The identified chemical species mass concentrations can explain 79±3%, 82±6% and 57±6% of the total particle mass in the condensation, droplet and coarse mode, respectively. Organic matter (OM) and elemental carbon (EC) in the condensation mode, OM, $(NH_4)_2SO_4$, NH_4NO_3 and crustal element oxides in the droplet mode, and crustal element oxides, OM and $CaSO_4$ in the coarse mode were the dominant chemical species in their respective modes. The measured b_{sp} can be reconstructed to the level of 91±10% using Mie theory with input of the estimated chemically-resolved number concentrations of NaCl, $NaNO_3$, Na_2SO_4, NH_4NO_3, $(NH_4)_2SO_4$, K_2SO_4, $CaSO_4$, $Ca(NO_3)_2$, OM, EC, crustal element oxides and unidentified fraction. MSEs of particle and individual chemical species were underestimated by less than 13 % in any season based on the estimated b_{sp} and chemical species mass concentrations. Seasonal average MSEs varied in the range of 3.5±0.1 to 3.9±0.2 $m^2\ g^{-1}$ for fine particles (aerodynamic diameter smaller than 2.1 μm), which was mainly caused by seasonal variations of the mass fractions and MSEs of the dominant chemical species (OM, NH_4NO_3, $(NH_4)_2SO_4$) in the droplet mode. MSEs of the dominant chemical species were determined by their log-normal size distribution parameters including MMADs and standard deviation (σ) in the droplet mode.

Keywords: particle size distribution, particle chemical composition, particle mass scattering efficiency

1. Introduction

Light extinct coefficient (b_{ext}) of atmospheric particles, which is the sum of their scattering (b_{sp}) and absorption (b_{ap}) coefficients, is a key index of haze weather (Hand and Malm, 2007). In most cases, b_{sp} accounted for more than 90% of b_{ext} (Takemura et al., 2002; Tao et al., 2017a). Numerous studies have demonstrated that haze is mainly caused by high concentrations of fine particles ($PM_{2.5}$, with aerodynamic diameter smaller than 2.5 μm) (Hand and Malm, 2007; Huang et al., 2012; Malm et al., 1994; Malm et al., 2000; Malm et al., 2003; Malm and Hand, 2007; Sisler and Latimer, 1993; Sisler et al., 1996; Sisler and Malm, 2000; Wang et al., 2014; Zhao et al., 2013). Knowledge of the dominant chemical species in $PM_{2.5}$ (e.g. $(NH_4)_2SO_4$, NH_4NO_3 and OM) and their contributions to b_{sp} is crucial in making feasible policies for alleviating haze (Watson, 2002).

Generally, b_{sp} can be estimated in reasonable accuracy using Mie theory when size distributions of the dominant chemical species are known (Cheng et al., 2008; Cheng et al., 2009; Gao et al., 2015; Malm et al., 2003; Watson et al., 2008). However, routinely monitoring of the size distributions of all the dominant chemical components is impractical. To evaluate haze in the national parks in U.S.A. under the Regional Haze Rule, the original and revised empirical formulas from the Interagency Monitoring of Protected Visual Environments (IMPROVE) network were developed for reconstructing b_{sp} based on the chemical species in $PM_{2.5}$ and coarse particle mass concentrations monitored in the IMPROVE network (Pitchford et al., 2007; Watson, 2002). MSEs of the chemical species are important parameters not only for building the

relationships between chemical species and b_{sp} (Hand and Malm, 2007), but also for relating particle mass to its optical properties (Lin et al., 2015; Titos et al., 2012). The recommended MSEs of $(NH_4)_2SO_4$, NH_4NO_3, OM and fine soil (estimated from crustal elements) in $PM_{2.5}$ were 3.0, 3.0, 4.0 and 1.0 $m^2\ g^{-1}$, respectively, in the original IMPROVE formula based on the assumed size distributions. However, MSE of any particle species vary with its mass concentration and size distribution (Lowenthal and Kumar, 2004; Malm et al., 2003; Malm and Hand, 2007; Malm and Pitchford, 1997). Subsequently, MSEs and mass concentrations of $(NH_4)_2SO_4$, NH_4NO_3 and OM in $PM_{2.5}$ were separated into small and large modes in the revised IMPROVE formula (Hand and Malm, 2007).

China has been suffering from severe $PM_{2.5}$ pollution and haze weather (Li et al., 2016; Ming et al., 2017; Wang et al., 2017; Zhang et al., 2013). To investigate the formation of haze, the original and revised IMPROVE formulas have been directly applied in many cities in China (Hua et al., 2015; Shen et al., 2014; Tao et al., 2009; Zhang et al., 2012a; Zou et al., 2018). The IMPROVE formulas have been proved to over- or underestimate b_{sp} in urban cities in China (Cao et al., 2012; Cheng et al., 2015; Han et al., 2014; Jung et al., 2009a; Jung et al., 2009b; Tao et al., 2012; Tao et al., 2014), which were likely due to the significantly different size distributions of the major chemical components and related mass fractions in $PM_{2.5}$ between different countries or even cities (Bian et al., 2014; Cabada et al., 2004; Chen et al., 2017; Guo et al., 2009; Lan et al., 2011; Tian et al., 2014; Yao et al., 2003; Yu et al., 2010; Zhang et al., 2008; Zhuang et al., 1999b). To reduce the uncertainties in the estimated b_{sp} using the original

and revised IMPROVE formulas, the average MSEs of the dominant chemical species were typically estimated by the multiple linear regression method (Hand and Malm, 2007). Although the estimated b_{sp} by the multiple linear regression model may be close to the measured b_{sp}, the rationality of the estimated MSEs of chemical species were unknown.

Variations in size distributions of the chemical components (e.g., MMADs and mass fractions) are important factors for hindering the application of the IMPROVE formulas and multiple linear regression models. Although many studies have focused on size distributions and chemical compositions of fine particles in China, few studies have explored the relationship between the size distribution of major chemical species and their MSEs (Cheng et al., 2008; Cheng et al., 2009; Gao et al., 2015). To fill this knowledge gap, size-segregated particle mass, PM_{10}, $PM_{2.5}$ and their major chemical components, and inline data including size distribution of particle number, b_{sp} under dry condition and water-soluble inorganic ions were synchronously measured at an urban site in Guangzhou covering four seasons in 2015-2016. Size distributions of dominant chemical components were first characterized in section 3.1, followed by discussions on the closures of particle mass and number concentration and b_{sp} in 3.2. Key factors controlling the variations of chemical species and their MSEs were then discussed in section 3.3. Knowledge gained from the present study will improve the assessments of air-quality and climate impact caused by atmospheric particles, especially in urban areas.

2. Methodology

2.1 Site description

The observational site in urban Guangzhou is situated inside the South China Institute of Environmental Science (SCIES) (23°07′N, 113°21′E) (Fig. 1) with no obvious surrounding industrial activities. The instruments used in this study were installed on the roof of a building 50 m above ground (Tao et al., 2018). The working conditions of all the instruments were controlled under 26 degree in temperature and 40% in relative humidity (RH) by three air conditioners.

Insert Figure 1

2.2 Field sampling

Size-segregated particle samples were collected using Anderson 8-stage air samplers with the cut-off points of 0.43, 0.65, 1.1, 2.1, 3.3, 4.7, 5.8 and 9.0 μm (Thermo-electronic Company, USA). Two sets of samplers were used alternatively due to the need of daily clearance of the instruments. The samplers were operated at an airflow rate of 28.3 L min^{-1}. The sampling flow rate was controlled by a flow meter (Aalborg Inc., USA). Samples were collected on 81 mm quartz fiber filter (Whatman QM-A). Samples were collected during different seasons: 15 July- 6 August, 2015 (representative of summer), 15 October- 5 November, 2015 (autumn), 4-20 January, 2016 and 19-22 February, 2016 (winter), and 8-20 April, 2016 and 4-14 May, 2016 (spring). Sampling duration was 48 h in spring and 24 h in the other seasons, all starting at 10:00 local time.

Bulk $PM_{2.5}$ and PM_{10} samples were collected using two Gravisol Sequential Ambient Particulate Monitor (GSAPM) samplers (APM Inc., Korea) at a flow rate of

16.7 L min^{-1}. Samples were collected on 47 mm quartz fiber filter (Whatman QM-A). Sampling durations were the same as those for collecting size-segregated samples in every season. The sampling information is summarized in Table 1. Moreover, 8 sets of blank samples were also collected for each of the size-segregated particle, $PM_{2.5}$ and PM_{10} samples during the whole sampling period. Two sets of blank filters in each category were put in the samplers without flow for 24 h when seasonal field campaigns finished. The aerosol-loaded filter samples were stored in a freezer at -18 °C before analysis to prevent volatilization of particles.

Insert Table 1

The blank water-soluble inorganic ions (WSII) (e.g. Na^+, Ca^{2+}) of quartz fiber filter were slightly high in general. Thus, 47mm and 81mm quartz fiber filters were first baked at 500 °C for 3 h to remove adsorbed organic vapors; they were then soaked in distilled-deionized water for 3 h for several times to remove WSII until the background values were less than 0.01 mg L^{-1}. Finally, the quartz fiber filters were dried through baking at 200 °C. All blank quartz fiber filters were stored in desiccators.

Particle number concentration for particles in the range of 14 nm - 615 nm in mobility diameter (D_p) was measured using a scanning mobility particle sizer (SMPS; TSI Model 3936, TSI, Inc., St. Paul, MN) combined with a long differential mobility analyzer (DMA; TSI Model 3080) and a condensation particle counter (CPC; TSI Model 3010), and for particles in the range of 542 nm - 10 μm aerodynamic diameter (D_a) using an Aerodynamics Particle Sizer (APS; TSI Model 3321), both at 5 min resolution. APS was calibrated using 5 sizes solid spheres (polystyrene latex monodisperse). Dry b_{sp} was measured using a single wavelength integrating

nephelometer (Ecotech Pty Ltd, Australia, Model Aurora1000G) at the wavelength of 520 nm at 5 min resolution. Zero calibration was performed every day with zero air, and span check was done every 3 days using HFC-R134a gas.

To exclude the impact of particle hygroscopic growth on the measured size distribution and b_{sp}, ambient air is forced to pass through three total suspended particulate (TSP) cyclones, then stainless steel tubes and the Nafion driers prior to be sampled by the SMPS, APS and nephelometer. According to the method described in Kulkarni et al. (2011), particle losses in different sizes from the tube are plotted in Fig. S1. Generally, particle losses in the condensation (0.1-0.4 μm), droplet (0.4-2.1 μm) and coarse modes (2.1-10 μm) were less than 1.3%, 0.3% and 0.1%, respectively, suggesting that the particle losses from the tube were minimal. Ambient RH and temperature were measured by an automatic meteorological station (Vaisala Company, Helsinki, Finland, model MAWS201) at the SCIES site, and the seasonal average of these two meteorological parameters were 53-75 % and 15-29 °C, respectively. RH of aerosol samples was controlled to be lower than 30% by sweeping dry air from a compressed air pump. NO_3^- was measured using an In-situ instrument of Gas and Aerosol Composition (IGAC, Model S-611, Machine Shop, Fortelice International Co., Ltd., Taiwan, China) at a resolution of 1-h (Tao et al., 2018).

2.3 Lab chemical analysis and data quality assurance and control

47 mm and 81 mm quartz fiber filters were measured gravimetrically for particle mass concentration using a Sartorius ME 5-F electronic microbalance with a sensitivity of ±1 μg (Sartorius, Göttingen, Germany) after 24 h equilibration at temperature of 23±1 °C and RH of 40±5%. Microbalance was calibrated by 5 mg, 200 mg and 5000 mg weights before weighting. Each filter was weighed at least three times before and after sampling. Differences among replicate weights were mostly less than 20 μg for

each sample. Net mass was obtained by subtracting pre-weight from post-weight.

Three pieces of 0.526 cm^2 punches from each 47 mm quartz filter samples and one-fourth of each 81 mm quartz filter samples were used to determine water-soluble inorganic ions. The extraction of water-soluble species from each filter was put into a separate 4 mL bottle, followed by 4 mL distilled-deionized water (with a resistivity of >18 MΩ), and then subjected to ultrasonic agitation for 1 h for complete extraction of the ionic compounds. The extract solutions were filtered (0.25 μm, PTFE, Whatman, USA) and stored at 4 °C in pre-cleaned tubes until analysis. Cation (Na^+, NH_4^+, K^+, Mg^{2+} and Ca^{2+}) concentrations were determined by ion chromatography (Dionex ICS-1600) using a CS12A column with 20 mM Methanesulfonic Acid eluent. Anions (SO_4^{2-}, NO_3^-, Cl^-, and F^-) were separated on an AS19 column in ion chromatography (Dionex ICS-2100), using 20 mM KOH as the eluent. A calibration was performed for each analytical sequence. Procedural blank values were subtracted from sample concentrations. Method detection limits (MDL) of ions were within the range of 0.001 to 0.002 mg L^{-1}.

OC and EC were analyzed using a DRI model 2001 carbon analyzer (Atmoslytic, Inc., Calabasas, CA, USA). An area of 0.526 cm^2 punched from each 47mm quartz filter and 1-4 dots punched from each 81mm quartz filter were analyzed for four OC fractions (OC1, OC2, OC3, and OC4 at 140 °C, 280 °C, 480 °C, and 580 °C, respectively, in a helium [He] atmosphere); OP (a pyrolyzed carbon fraction determined when transmitted laser light attained its original intensity after oxygen [O_2] was added to the analyzed atmosphere); and three EC fractions (EC1, EC2, and EC3 at 580 °C,

740 °C, and 840 °C, respectively, in a 2% O_2/98% He atmosphere). Here, OC is operationally defined as OC1 + OC2 + OC3 + OC4 + OP and EC is defined as EC1 + EC2 + EC3 – OP for 47mm samples. However, OC is operationally defined as OC1 + OC2 + OC3 + OC4 and EC is defined as EC1 + EC2 + EC3 for 81mm samples due to extremely low OP level. Average field blanks were subtracted from each sample filter. MDLs of OC and EC were 0.41±0.2 μgC cm^{-2} and 0.03±0.2 μgC cm^{-2}, respectively.

To obtain high quality data of the size distributions of major chemical components, bulk $PM_{2.5}$ and PM_{10} samples were synchronously collected and the same chemical components were analyzed. Generally, good correlations (R^2>0.90) were found in the mass concentrations of the total particle and major chemical components (including total carbon (TC), NO_3^- and SO_4^{2-}) between the size-segregated samples (PM_{10} and $PM_{2.1}$) and the GSAPM samplers (PM_{10} and $PM_{2.5}$). The regression slopes were in the range of 0.91- 1.05, suggesting good and acceptable data quality of the size distributions of the major chemical components (Fig.S2).

2.4 Data analysis methods

The ISORROPIA II model was run at the reserved mode (Fountoukis and Nenes, 2007) with input data of K^+, Ca^{2+}, Mg^{2+}, NH_4^+, Na^+, SO_4^{2-}, NO_3^-, Cl^-, RH (40%), and temperature (25°C), to estimate the size-resolved mass concentrations of NaCl, $NaNO_3$, Na_2SO_4, $NaHSO_4$, NH_4Cl, NH_4NO_3, $(NH_4)_2SO_4$, NH_4HSO_4, K_2SO_4, $KHSO_4$, KNO_3, KCl, $MgSO_4$, $Mg(NO_3)_2$, $MgCl_2$, $CaSO_4$, $Ca(NO_3)_2$, $CaCl_2$ and H_2O. Several of these chemical species had extremely low mass concentrations and were thus excluded from the calculation of b_{sp}. Generally, only NaCl, $NaNO_3$, Na_2SO_4, NH_4NO_3, $(NH_4)_2SO_4$, K_2SO_4, $Ca(NO_3)_2$, $CaSO_4$ and H_2O were used to estimate b_{sp} in this study.

In this work, the cut-off point of 2.1 μm was chosen to separate the fine and coarse mode particles for investigating the impact of aerosol size distribution on their

respective MSEs. Moreover, the cut-off sizes of <0.43 μm and 0.43 - 2.1 μm were used to separate the condensation mode and droplet mode, respectively. Particle MSE was estimated by the sum of b_{sp} from individual chemical species divided by sum of particle mass concentration according to:

$$MSE = \frac{\int_0^{D_{i,j}^{max}} b_{sp}\ dD_{i,j}}{\int_0^{D_{i,j}^{max}} C\ dD_{i,j}} \quad (1)$$

Where i is chemical species, j is chemical species size, $D_{i,j}$ is the chemical species diameter, and C is chemical species mass concentration.

b_{sp} was estimated by the Mie model as follows:

$$b_{sp} = \int_0^{D_{i,j}^{max}} \frac{\pi}{4} D_{i,j}^2 Q_{sp}(m_{i,j}, D_{i,j}, \lambda) N_{i,j} dD_{ij} \quad (2)$$

Where Q_{sp} is single-particle scattering efficiency of chemical species (Fig. S3), $m_{i,j}$ is refractive index of chemical species (Table S1), λ is 550 nm, and $N_{i,j}$ is number concentration of chemical species calculated by the formula (3).

$$N = \frac{6C}{\pi \rho D^3} \quad (3)$$

Where N is chemical species number concentration, C is chemical species mass concentrations, ρ is density of chemical species (Table S1), and D is geometric diameter (D_g) of chemical species.

The particle number concentration in aerodynamic diameter (D_a) was converted to the particle number concentration in D_g (similar to D_p) according to:

$$D_a = D_g/(\rho)^{0.5} \quad (4)$$

$$\rho = \frac{\sum_{chemical\ species} m_i}{\sum_{chemical\ species} \frac{m_i}{\rho_i}} \quad (5)$$

Where ρ represents the daily average density of particle, i is chemical species, m_i

is chemical species mass concentration in a bin, and ρ_i is chemical species density. The seasonal average densities of particle are shown in Fig. S4.

Continuous size-distribution profiles of major chemical species are needed in order to accurately calculate b_{sp} using Mie theory. To improve the resolution of b_{sp}, 401 bins were used for chemical species ranging from 10 nm to 100 μm, with a constant ratio between the adjacent size bins, defined as $\log_{10}(D_{a2}/D_{a1})=0.01$. Further increasing the number of size bins does not have any significant impact on the results, e.g., the changes in b_{sp} are smaller than 1% even if the above ratio of 0.01 is replaced with 0.001. Continuous size-distribution profiles of major chemical species are obtained from the inversion of the measured mass concentration distribution in the size bins of the Anderson 8-stage air samplers, using the technique described in Dong et al. (2004). The key formulas to calculate the normal distribution of density function (f (D, μ, σ)) were summarized as follows:

$$f(D,\mu,\sigma)=\frac{1}{\sqrt{2\pi}\sigma}e^{-\left(\frac{(D-\mu)^2}{2\sigma^2}\right)} \quad (6)$$

$$\mu=\bar{y}-\mu\bar{x} \quad (7)$$

$$\sigma=\frac{n\sum xy-\sum x\times\sum y}{n\sum x^2-(\sum x)^2} \quad (8)$$

Where D is log (D_a), and μ and σ are the mean and standard deviation, respectively, of the log (D_a) in the different modes. x is the inverse function value of the cumulative probability of a standard normal distribution in each bin, y is logarithm of D_a lower limit (e.g. 0.43, 0.65, 1.1, 2.1, 3.3, 4.7, 5.8 and 9.0 μm) in each bin. An example of the calculation process was demonstrated in supplementary.

However, this approach is not applicable for the condensation mode because there is only one size bin in this mode. To obtain the number concentrations of all the concerned chemical species in the condensation mode, MMADs ($=10^{\mu}$) of this mode are calculated according to:

$$MMADs = (D_{a1} \times D_{a2})^{0.5} \quad (9)$$

Where D_{a1} and D_{a2} represent the lower (0.10 μm, limits of detection of Anderson 8-stage air sampler) and upper (0.43 μm) boundaries of this size bin, respectively.

3. Results and Discussion

3.1 Size distributions of total particle mass and major chemical components

3.1.1 Total particle mass

Generally, any particle size distribution can be fitted into a combination of condensation, droplet and coarse modes (John et al., 1990). Continuous log-normal size distributions of particle mass including the condensation, droplet and coarse modes were calculated using the method described in section 2.4 and are summarized in Table 2. On annual average, 10±2%, 48±7% and 42±8% of total mass in the size-segregated samples were in the condensation, droplet and coarse modes, respectively, with the average MMADs being 0.78±0.07 μm in the droplet mode and 4.57±0.42 μm in the coarse mode. These values were comparable to those observed by the Micro-Orifice Uniform Deposit Impactor (MOUDI) in the other cities (e.g. Shenzhen and Hong Kong) of the Pearl River Delta (PRD) region (Bian et al., 2014; Lan et al., 2011; Yu et al., 2010).

The estimated annual $PM_{2.5}$ concentration based on the continuous log-normal size distribution was 36.4±13.2 μg m^{-3}, which was close to the synchronously measured $PM_{2.5}$ (36.8±15.3 μg m^{-3}), although slightly higher than the sum of the mass concentrations (34.9±13.8 μg m^{-3}) in the condensation and droplet modes. Thus, the fine (sum of condensation and droplet) mode particles can reasonably represent $PM_{2.5}$. Seasonal average particle mass concentrations were evidently lower in summer than in the other seasons for the condensation and droplet modes, and were similar during spring, autumn and winter for all the three modes. These results agree with the seasonal

287 variations of $PM_{2.5}$ observed at the same site in 2009-2010 (Tao et al., 2014).

288

289 *Insert Table 2*

290

291 **3.1.2 Water-soluble inorganic ions**

292 Generally, SO_4^{2-}, NO_3^- and NH_4^+ are the dominant WSIIs, especially in the
293 condensation and droplet modes. They are mainly formed through aqueous-phase
294 reactions in moisture conditions in the PRD region (Lan et al., 2011; Yu et al., 2010).
295 As expected, 77±6% SO_4^{2-}, 46±16% NO_3^- and 89±7% of NH_4^+ mass concentrations
296 were in the droplet mode on annual average due to their aqueous-phase formations
297 (Table 2). Much lower fractions for NO_3^- than SO_4^{2-} and NH_4^+ in the droplet mode
298 were mostly due to the high volatility of NH_4NO_3 (Zhang et al., 2008). The MMADs
299 of the three ions in the droplet mode were in the range of 0.70-0.94 μm, comparable
300 with MOUDI measurements (0.78-1.03 μm) conducted in the PRD region (Bian et al.,
301 2014; Lan et al., 2011; Yu et al., 2010).

302 Small fractions of SO_4^{2-}, NO_3^- and NH_4^+ masses were distributed in the
303 condensation mode, e.g., 12±4%, 10±4% and 6±5%, respectively, on annual average.
304 The mass fractions of SO_4^{2-} in the condensation mode shown above were much lower
305 than those (24-29%) observed in urban Guangzhou in 2006-2007 (Yu et al., 2010),
306 suggesting gas-phase chemical reactions of SO_2 has become less important in the
307 formation of SO_4^{2-}, likely due to the dramatic reduction of SO_2 emissions in urban or
308 suburban Guangzhou in the recent decade (Zheng et al., 2009; Zheng et al., 2018).

309 11±5% SO_4^{2-}, 44±18% NO_3^- and 5±4% of NH_4^+ mass concentrations were
310 distributed in the coarse mode. In general, NO_3^- mainly exists in the form of NH_4NO_3
311 in the condensation and droplet modes and associates with base cations in the coarse

mode (e.g., $Ca(NO_3)_2$ and $NaNO_3$) (Zhang et al., 2015a). More than 50% NO_3^- mass concentrations were distributed in the coarse mode in summer and autumn when ambient temperatures were high. The MMADs of NO_3^- in the coarse mode were 4.15±0.52 and 4.36±0.31 μm in summer and autumn, respectively, slightly lower than those of Ca^{2+} (4.10±0.42 and 4.72±0.47 μm in the same seasons), but evidently higher than those of Na^+ (3.60±0.19 and 3.64±0.27 μm) (Table 2). This suggests that NH_4NO_3 was prone to dissociate to $HNO_{3(g)}$ in summer and autumn due to the high ambient temperatures with released $HNO_{3(g)}$ further reacting with mineral dust and to a less extent with sea salt particles. In comparison, the MMADs of SO_4^{2-} in the coarse mode were in between of those of Ca^{2+} and Na^+, likely due to uptake of $H_2SO_{4(g)}$ by both mineral dust and sea salt particles (Zhang et al., 2015a). In contrast, the MMAD of NH_4^+ in the coarse mode was 3.25±0.69 μm, much smaller than those of SO_4^{2-} and NO_3^-, suggesting that NH_4^+ in the coarse mode was likely from hygroscopic growth of NH_4^+ in the droplet mode (Tian et al., 2014).

It is also worth mentioning that most of Cl^- was distributed in the coarse mode and its MMAD (3.77±0.35 μm) was very close to that of Na^+ (3.75±0.38 μm), especially in summer when air masses were originated from the China South Sea (Tao et al., 2017b; Xia et al., 2017). The mole ratios of Cl^-/Na^+ were less than 1.0 in all the seasons but spring due to the reactions between sea salt and acid gasses ($HNO_{3(g)}$ and $H_2SO_{4(g)}$) (Zhuang et al., 1999a). The excess Cl^- in the coarse mode in spring was likely due to the aged biomass burning particles from the southeast Asian (Zhang et al., 2015c). In fact, the concentration of the typical biomass burning tracer K^+ in the coarse mode was higher in spring than in the other seasons (Fig. S5). In any case, sea salt was mainly distributed in the coarse mode rather than the droplet mode in urban Guangzhou.

3.1.3 OC and EC

OC and EC in fine particles can be produced from both primary emissions of vehicle exhaust, coal combustion, biomass burning and secondary formation (Chow et al., 2011; Gentner et al., 2012; Gentner et al., 2017; Hallquist et al., 2009; Zheng et al., 2006). In general, fresh OC and EC particles emitted from vehicle exhaust, coal combustion and biomass burning should be distributed in the condensation mode (Schwarz et al., 2008; Zhang et al., 2012b). Only 13±4% of OC and 31±7% of EC mass concentrations were distributed in the condensation mode in the present study (Table 2). OC/EC ratios were in the range of 0.9-1.6 in the condensation mode, suggesting that vehicle exhaust was the dominant source of OC and EC in this particle size range (Huang et al., 2006a; Schwarz et al., 2008; Shiraiwa et al., 2007; Watson et al., 2001; Wu et al., 2017). 62±9% of OC and 55±7% of EC mass concentrations were distributed in the droplet mode (Table 2), similar to that of SO_4^{2-}. These numbers were similar to those observed in the other cities of the PRD region, and was previously identified to be mainly caused by in-cloud aerosol processing (Huang et al., 2006b). Cloud processing indeed plays important roles in forming droplet mode aerosols in urban Guangzhou (Tao et al., 2018). OC/EC ratios were in the range of 2.2-3.2 in the droplet mode, much higher than those in the condensation mode, suggesting that OC in the droplet mode was mainly aged or secondary particles (Day et al., 2015; Huang et al., 2006a; Wu and Yu, 2016).

The MMADs of OC and EC in the droplet mode were 0.76±0.07 μm and 0.66±0.08 μm, respectively, which were slightly lower than those (0.7-1.0 μm for OC and 0.8-1.0 μm for EC) found in earlier studies in the PRD region (e.g. Guangzhou, Hong Kong and Shenzhen) (Lan et al., 2011; Yu et al., 2010). Noticeably, the MMADs of OC and EC in the droplet mode were very close to those (0.73 μm for OC and 0.77

μm for EC) measured in summer at a suburban site of Hong Kong, where the loadings of the dominant chemical components (e.g. OC, EC and SO_4^{2-}) were low (Yu et al., 2010).

Road dust and biogenic aerosols were generally considered as the major sources of OC and EC in the coarse mode (Ho et al., 2003; Zhang et al., 2015b). Significant fractions of OC (25±8%) and EC (14±7%) mass concentrations were distributed in the coarse mode. These numbers were comparable with those (13-38% for OC and 4-16% for EC) measured at suburban sites of Guangzhou, Shenzhen and Hong Kong (Lan et al., 2011; Yu et al., 2010), but were lower than those (51-57% for OC and 17-21% for EC) measured in urban Guangzhou in 2006-2007. The MMADs of OC (3.73±0.58 μm) and EC (3.69±0.65 μm) in the coarse mode were close to those (3.8-4.3 μm for OC and 3.7-4.1 μm for EC) measured in suburban of Hong Kong, although smaller than those (4.8-5.2 μm for OC and 5.0-5.2 μm for EC) measured in suburban of Shenzhen and urban of Guangzhou (Lan et al., 2011; Yu et al., 2010). These results suggested that the MMADs of OC and EC might decrease with their decreasing coarse mode mass fractions. Annual average PM_{10} concentrations (46 μg m^{-3}) in 2015-2016 in the PRD region were about 40% lower than that (76 μg m^{-3}) in 2006-2007, which further supported the above hypothesis.

3.2 Closure of particle mass, number concentration, and b_{sp}

3.2.1 Closure of particle mass concentration

To investigate the impact of chemical species in different size modes on b_{sp}, particle mass concentrations in the different modes were first reconstructed based on mass concentrations of individual known chemical components. The dominant water-soluble inorganic species including NaCl, $NaNO_3$, Na_2SO_4, NH_4NO_3, $(NH_4)_2SO_4$, K_2SO_4, $CaSO_4$ and $Ca(NO_3)_2$ were determined using the ISORROPIA II

386 thermodynamic equilibrium model as mentioned in section 2.4. A ratio of OM to OC
387 of 1.4, 1.6 and 1.6 would be appropriate for the condensation, droplet and coarse mode,
388 respectively, which was based on the findings of a previous study that suggested an
389 average OM/OC ratio of 1.57 and a range of 1.4-1.8 in an urban environment of the
390 PRD region (He et al., 2011). In our previous study (Tao et al., 2017b), mass
391 concentration of crustal element oxides in $PM_{2.5}$ was estimated from the measurements
392 of five crustal elements (Al, Si, Ca, Fe and Ti) in urban Guangzhou. This approach
393 cannot be used in the present study due to the lack of crustal elements measurements.
394 Alternatively, crustal element oxides mass concentration was estimated from Ca^{2+} mass
395 concentration because of their good correlations (slope=0.053, R^2=0.79) as was found
396 in a previous study (Fig. S6) (Tao et al., 2017b). It was suggested that Ca^{2+} accounted
397 for 5.3% of crustal element oxides in $PM_{2.5}$ in urban Guangzhou, a value that is close
398 to the content of Ca^{2+} (5.0%) in soil dust source profiles (representing crustal element
399 oxides) in $PM_{2.5}$ in cities of southern China (Sun et al., 2019). Because $CaSO_4$ and
400 $Ca(NO_3)_2$ were mainly from the reactions between calcium oxide and acids (e.g.
401 H_2SO_4 and HNO_3), the estimated mass concentration of crustal element oxides needs
402 to deduct those of $CaSO_4$ and $Ca(NO_3)_2$. On annual average, the estimated crustal
403 element oxides accounted for 8±2%, 10±4% and 29±5% of the total particle mass
404 concentrations in the condensation, droplet and coarse mode, respectively. The
405 reconstructed mass concentrations accounted for 79±3%, 82±6% and 57±6% of the
406 total in the condensation, droplet and coarse mode, respectively.

407 As shown in Fig. 2, OM, EC, $(NH_4)_2SO_4$, NH_4NO_3 and crustal element oxides
408 dominated in different modes in four seasons. For example, OM and EC accounted for
409 31-39% and 14-19%, respectively, of particle mass in the condensation mode, OM,
410 $(NH_4)_2SO_4$, crustal element oxides and NH_4NO_3 accounted for 19-34%, 18-22%, 6-

15% and 4-11%, respectively, in the droplet mode, and crustal element oxides, OM and $CaSO_4$ accounted for 22-34%, 12-17% and 4-5%, respectively, in the coarse mode. In addition, the total of the other identified chemical species only accounted for less than 10% of the total particle mass in every mode. For example, Na_2SO_4 and K_2SO_4 mainly distributed in the droplet mode and together they accounted for only 2-5% of the particle mass in this mode. NaCl, $NaNO_3$ and $Ca(NO_3)_2$ mainly distributed in the coarse mode and each of these species accounted for less than 2% of the total particle mass in this mode.

Insert Figure 2

3.2.2 Closure of particle number concentration

To estimate the contribution of individual chemical species on b_{sp} using Mie theory, number size distributions of the dominant chemical species were needed and were calculated according to the method described in section 2.4. As shown in Fig. 3, most chemical species (except $(NH_4)_2SO_4$ in summer) had much higher number concentrations in the condensation than droplet or coarse mode. The estimated number mean aerodynamic diameters (NMADs) of the number concentrations of individual chemical species mainly distributed in the range of 100-120 nm. The estimated NMADs of particle number concentrations (sum of individual chemical species number concentrations in the same size bin) were close to about 100 nm in the four seasons, which was larger than the NMADs (30-70 nm) of the simultaneously measured particle number concentrations by the SMPS and APS (Fig. 4). This was because SMPS and APS collected dried particles while the size-segregated sampler collected ambient particles. D_p of particles measured by SMPS can be converted to D_a using the average

436 particle density calculated from the synchronously measured size-segregated individual
437 chemical species mass concentrations and densities according to the method described
438 in section 2.4. In any case, the NMADs of particle number concentrations were less
439 than 100 nm regardless of using SMPS and APS measurements or the estimated size-
440 segregated chemical species mass concentrations.

441 As shown in Fig. 3 and Fig. 4, most of particle numbers were in the range of 10 -
442 400 nm either observed by the SMPS or estimated from the size-segregated chemical
443 species mass concentrations. Total particle number concentration in the range of 10 nm-
444 10 μm measured by the SMPS and APS were 7038±2250 cm^{-3}, 9774±1471 cm^{-3},
445 5694±1942 cm^{-3} and 10801±2986 cm^{-3} in spring, summer, autumn and winter,
446 respectively, which were 1.09±0.24, 2.66±0.48, 1.05±0.20 and 2.33±0.67 times of those
447 estimated by the size-segregated chemical species mass concentrations.

448 NMADs estimated from the size-segregated chemical species mass concentrations
449 were close to those measured by the SMPS and APS in spring and autumn, resulting in
450 the close estimation of particle number concentrations to the measured ones. In contrast,
451 the estimated particle number concentrations from the the size-segregated chemical
452 species mass concentrations were evidently lower than those measured by the SMPS
453 and APS in summer and winter, due to the much higher NMADs (100 nm) estimated
454 from the size-segregated chemical species mass concentrations than those (about 30 or
455 40 nm) measured by the SMPS and APS.

456 To exclude the large uncertainties in the estimated particle number concentration
457 caused by condensation mode particles (which were due to the design flaws of size-
458 segregated sampler), particles smaller than 430 nm were not included in the calculation
459 below. On annual average, the estimated particle number concentrations in the range of
460 430 nm-10 μm based on the size-segregated chemical species mass concentrations were

33±42% higher than those measured by the SMPS and APS. This was likely because particles in the droplet mode may shift to the smaller sizes (<430 nm) during the dry process by Nafion tube. Correlation coefficients between the estimated and measured particle number concentrations in the range of 430 nm-10 μm were significantly improved when the intercepts in the linear regression equations were retained. To some extent, the intercepts represent the measurement errors of SMPS and APS and estimation errors of the inversion technique and ISORROPIA II models. In any case, good correlations (R^2>0.81) between the estimated daily particle number concentrations and the measured ones were found and the slopes ranged from 0.79 to 1.03 in the four seasons (Fig. 5). These results suggested that the estimated particle number concentrations were acceptable in the range of 430 nm-10 μm, noting that particles in this size range dominate particle scattering efficiency.

Insert Figure 3

Insert Figure 4

Insert Figure 5

3.2.3 Closure between the measured and estimated b_{sp}

Daily b_{sp} was estimated using Mie model (in section 2.4) with input parameters including refractive indices, densities and number concentrations in 401 bins of chemical species (NaCl, $NaNO_3$, Na_2SO_4, $(NH_4)_2SO_4$, NH_4NO_3, K_2SO_4, $CaSO_4$, $Ca(NO_3)_2$, H_2O, OM, EC, crustal element oxides and unidentified fraction). The refractive indices and densities of above chemical species are summarized in Table S1. Although the number concentrations in the condensation mode were underestimated,

good correlations (R^2> 0.92) were found between the measured and estimated b_{sp} with the slopes being 0.87, 0.87, 0.85 and 0.89 in spring, summer, autumn and winter, respectively (Fig. 6). On annual arithmetic average, the estimated b_{sp} can explain 91±10% of the measured b_{sp}. The residual fractions were likely related to the chosen convert factor between OM and OC, measurements and sampling errors of chemical species (especially NO_3^-), errors from the models (ISORROPIA II model, Mie model, and the inversion technique method), and measurement errors caused by the size-segregated sampler (Vaughan, 1989). Magnitudes of the uncertainties caused by these sources are discussed below.

Although the convert factor of 1.6 between OM and OC was reasonable in urban environment, a value of as high as 1.8 was found in literature (He et al., 2011). In addition, OC mass concentrations were likely underestimated due to the OC/EC protocol for size-segregated samples. Nevertheless, the estimated b_{sp} can only be increased by less than 3% if increasing the convert factor to 1.8 in the droplet mode. Note that a previous study at the Fresno Supersite increased the estimated b_{sp} by about 10% when increasing the convert factor from 1.4 to 1.8, likely due to the high mass fraction of OC in fine particle at this site (Watson et al., 2008).

Different from the other chemical species, NH_4NO_3 can dissociate into $HNO_{3(g)}$ and $NH_{3(g)}$ during the filter gravimetric weighing process under dry condition. To evaluate the evaporative loss of NH_4NO_3, synchronous inline data of NO_3^- were also measured by an In-situ Gas and Aerosol Composition monitoring system at hourly temporal resolution (Fig. S7). Seasonal average NO_3^- concentrations were 42% ($PM_{2.5}$), 39% (PM_{10}), 42% ($PM_{2.5}$) and 19% ($PM_{2.5}$) less from filter measurements than inline measurements in spring, summer, autumn and winter, respectively. Adjusting the filter NO_3^- data using the above ratios can increase the estimated b_{sp} by 7%, 2%, 4% and 2%

511 in the respective season.

512

513 *Insert Figure 6*

514

515 Meanwhile, the measured b_{sp} could also be underestimated due to the
516 dissociation of NH_4NO_3 during the dry processes of ambient particles through the
517 Nafion dryer. A previous study indicated the measured b_{sp} being decreased by less
518 than 10% due to the dissociation of NH_4NO_3 in a heated nephelometer (Bergin et al.,
519 1997). In the present study, the chamber temperatures of nephelometer were less than
520 300 K and the particle residence time in both the Nafion dryer and the nephelometer
521 chamber was about 7 seconds. Thus, the bias in the measured b_{sp} should be less than
522 2% in any season according to the relationship among the loss of b_{sp}, residence time
523 and the temperature in chamber in a previous study (Bergin et al., 1997). Combining
524 all of the above-mentioned factors, the adjusted estimated b_{sp} would increase to the
525 level of 92%, 87%, 87% and 89% of the measured b_{sp} in spring, summer, autumn and
526 winter, respectively. This means the above methods for estimating b_{sp} were
527 reasonable with the adjusted estimated values explaining 87-92% of the measured
528 values after the filter-based NO_3^- concentrations were adjusted based on the inline
529 data. Thus, the errors from the models and size-segregated samplers may account for
530 the remaining 8-13% of the measured b_{sp}. Moreover, the size distributions would be
531 different under dry and ambient conditions due to the particle hygroscopic properties.
532 In fact, the NMADs of particle measured by SMPS and APS under dry condition
533 were less than those measured by the size-segregated sampler under ambient
534 condition according to section 3.2.2. Thus, the estimated b_{sp} based on size
535 distributions of chemical species would be systematically higher to some extent than

the measured b_{sp} under dry condition.

Generally, the estimated seasonal average b_{sp} were 146±40 Mm^{-1}, 99±33 Mm^{-1}, 169±54 Mm^{-1} and 151±71 Mm^{-1} in spring, summer, autumn and winter, respectively (Fig. 7). The particles in the condensation, droplet and coarse modes contributed 6-7%, 81-86% and 8-12%, respectively, to the estimated b_{sp}. OM and EC were the dominant contributors, accounting for 32-41% and 30-37%, respectively, of the estimated b_{sp} in the condensation mode. OM and secondary inorganic aerosols (sum of $(NH_4)_2SO_4$ and NH_4NO_3) were the dominant contributors, accounting for 27-44% and 27-34%, respectively, of the estimated b_{sp} in the droplet mode. Unidentified fraction, crustal element oxides and OM were the dominant contributors, accounting for 26-47%, 16-29% and 19-27%, respectively, of the estimated b_{sp} in the coarse mode. The sum of the dominant contributors, including OM, EC, secondary inorganic aerosols and crustal element oxides, accounted for 70-79% of the estimated b_{sp} in the four seasons. In contrast, the sum of the other chemical species (including NaCl, $NaNO_3$, Na_2SO_4, K_2SO_4, $CaSO_4$, $Ca(NO_3)_2$, H_2O) accounted for 5-10% and the unidentified fraction, 12-23% of the estimated b_{sp}. In conclusion, visibility degradation was determined by the dominant chemical species (e.g. OM, EC, secondary inorganic aerosols and crustal element oxides) in the fine mode (both condensation and droplet), which agreed with the results of the original and revised IMPORVE formulas (Pitchford et al., 2007).

Insert Figure 7

3.3 Key factors for variations of particle and chemical species MSEs

3.3.1 The estimated MSEs of particle and chemical species

To conveniently explore the control factors of particle MSE, the dominant chemical species' MSEs were estimated by their mass concentrations and the estimated b_{sp}, according to the measured chemical species mass concentrations in section 3.1 and the estimated b_{sp} in section 3.2. Here, only the MSEs of $(NH_4)_2SO_4$, NH_4NO_3, OM, EC, crustal element oxides and unidentified fraction in the condensation, droplet, fine (sum of condensation and droplet), and coarse modes were estimated (Table 3), considering these chemical species accounted for more than 90% of the estimated b_{sp}. However, particle MSEs in the condensation, droplet, fine and coarse modes were estimated by sum of b_{sp} from individual chemical species divided by sum of particle mass concentration according to formula (9). Moreover, an external mixing of individual chemical species was assumed in the estimation. Generally, good correlations (R^2> 0.79) were found between the measured and estimated b_{sp} using the average MSEs of chemical species in Table 3 with the slopes being 0.85, 0.84, 0.76 and 0.84 in spring, summer, autumn and winter, respectively (Fig. S8). Thus, the estimated MSEs of chemical species in Table 3 were underestimated.

Insert Table 3

Undoubtedly, the particle MSE should be also underestimated because the estimated b_{sp} was 11-15% less of the measured b_{sp} in four seasons, as discussed in section 3.2. The measured b_{sp} would be biased low by about 3% due to the evaporation of NH_4NO_3, while the NO_3^- mass concentrations based the filter measurements were biased low by 5%, 3%, 9% and 6% in spring, summer, autumn and winter, respectively.

584 Thus, the MSEs of NO_3^- would be underestimated by 9%, 13%, 6% and 5% in the
585 respective season in the real world. In conclusion, the MSEs of particle and chemical
586 species were underestimated by less than 13%.

587 On annual average, the estimated particle MSEs in the condensation, droplet and
588 coarse modes were 2.1±0.2 $m^2 g^{-1}$, 4.3±0.2 $m^2 g^{-1}$ and 0.5±0.0 $m^2 g^{-1}$, respectively. The
589 estimated particle MSE in the fine (sum of condensation and droplet) mode, similar to
590 $PM_{2.5}$) was 3.7±0.2 $m^2 g^{-1}$, which was slightly higher than the value of 3.5 $m^2 g^{-1}$
591 estimated in 2009-2010 in urban Guangzhou (Tao et al., 2014). Seasonal variations of
592 the estimated MSEs in the fine mode followed the sequence of winter (3.9±0.2 $m^2 g^{-1}$)
593 > autumn (3.8±0.2 $m^2 g^{-1}$) > summer (3.6±0.2 $m^2 g^{-1}$) > spring (3.5±0.1 $m^2 g^{-1}$).
594 Evidently, the estimated MSEs in the fine mode were slightly higher in autumn and
595 winter than spring and summer, which also agreed with the previous studies in urban
596 Guangzhou (Andreae et al., 2008; Jung et al., 2009a).

597 On annual average, the estimated MSEs of $(NH_4)_2SO_4$, NH_4NO_3, OM and crustal
598 element oxides (equal to fine soil in the IMPROVE formulas) in the fine mode were
599 4.4±0.8, 4.5±1.5, 4.6±0.3 and 2.6±0.1 $m^2 g^{-1}$, respectively, which were higher than those
600 (3.0, 3.0, 4.0 and 1.0 $m^2 g^{-1}$, respectively) from using the original IMPROVE formula
601 (Hand and Malm, 2007; Malm and Hand, 2007; Pitchford et al., 2007). As shown in
602 Table 3, the MSEs of $(NH_4)_2SO_4$, NH_4NO_3, OM and crustal element oxides in the fine
603 mode depended on their mass fractions in the droplet mode with high MSEs. In the
604 original IMPROVE formula, MSEs of these chemical species were estimated using the
605 multiple linear regression model according to the chemical components in $PM_{2.5}$ and
606 b_{sp} from IMPROVE network, noting that significant mass fractions of particle were in
607 the condensation mode at the regional sites of IMPROVE network and an urban site in
608 U.S.A. (Cabada et al., 2004; Hand et al., 2002; Malm et al., 2003). In contrast, in the

present study most mass fractions of the dominant chemical species (e.g. $(NH_4)_2SO_4$, NH_4NO_3 and OM) in the fine mode were distributed in the droplet rather than condensation mode. These results suggested the higher MSEs of $(NH_4)_2SO_4$, NH_4NO_3 and OM in the fine mode in this study were likely due to their significant mass fractions in the droplet mode. In fact, the MSE of fine soil in the IMPROVE formulas would represent the MSE of the bulk mode rather than the fine mode (Hand and Malm, 2007). The average MSEs of the bulk mode was 1.0±0.2 m^2 g^{-1} in this study, which was similar to that in the IMPROVE formulas.

On annual average, the estimated MSEs of $(NH_4)_2SO_4$, NH_4NO_3 and OM were 4.7±0.6, 4.8±0.9 and 5.3±0.2 m^2 g^{-1} in the droplet mode, and were 2.1±0.5, 2.3±0.8 and 2.7±0.1 m^2 g^{-1} in the condensation mode, respectively, which were lower than those in the large mode (similar to droplet mode) and were slightly lower than those in the small mode (similar to condensation mode) in the revised IMPROVE formula (Pitchford et al., 2007). Theoretically, the highest MSEs of $(NH_4)_2SO_4$, NH_4NO_3 and OM would be found at about 0.55 μm in geometric mass mean diameters (GMMD) at the wavelength 550 nm according to Mie theory. However, the MMADs of $(NH_4)_2SO_4$, NH_4NO_3 and OM were 0.76 - 0.80 μm (equal to about 0.60-0.64 μm in GMMD) in the droplet mode and were 0.21 μm (equal to about 0.16-0.18 μm in GMMD) in the condensation mode in this study, which were larger than 0.50 μm in GMMD in the large mode and were lower than 0.20 μm in GMMD in the small mode in the revised IMPROVE formula. Thus, the higher GMMDs in the droplet mode and the lower GMMDs of $(NH_4)_2SO_4$, NH_4NO_3 and OM in the condensation mode in this study likely resulted in their lower MSEs compared with those in the revised IMPROVE formula. In addition, the underestimated b_{sp} would also result in underestimating their MSEs in the condensation and droplet modes in this study.

Although the contribution of EC to b_{sp} was not considered in the IMPROVE formulas, its mass extinction efficiency (10 m^2 g^{-1}) considered both scattering and absorption abilities (Hand and Malm, 2007). In fact, the theoretical average mass absorption efficiency (MAE) of EC in fine particle was 7.5 m^2 g^{-1} at the wavelength 550 nm (Wu et al., 2016). Thus, mass extinction efficiency of EC was also about 10 m^2 g^{-1} in this study, suggesting the estimated EC MSEs were comparable with the IMPROVE formulas. The estimated MSEs of coarse particle was 0.5±0.0 m^2 g^{-1}, which was also comparable with the value of 0.6 m^2 g^{-1} in the IMPROVE formulas. Noticeably, sea salt was mainly distributed in the coarse mode rather than droplet mode in this study. In addition, the unidentified fraction with large mass fraction and the high MSE in the fine mode was not considered in the IMPROVE formulas, although it accounted for a significant contribution of the estimated b_{sp} in this study (Fig. 7). In conclusion, EC and unidentified fraction rather than sea salt should be considered in estimating b_{sp}, especially when EC and unidentified fraction accounted for significant mass fractions of fine particles.

3.3.2 Impact of size distribution on particle and chemical species MSE

As discussed in section 3.3.1, seasonal average MSEs in the coarse mode fluctuated in a small range of 0.4-0.5 m^2 g^{-1}, while those in the fine mode in a slightly larger range of 3.5-3.9 m^2 g^{-1}, but the percentage changes are in similar magnitudes (10-20%). Only variations of fine particle MSE were discussed below as an example. It is worth to mention that fine particle MSE increased with its mass concentrations in IMPROVE network (Lowenthal and Kumar, 2004), but such a phenomenon was not founded in the present study. As shown in Fig. 8, the seasonal variations of fine particle MSE were mainly caused by particle fractions in the size range of 0.4-0.9 μm, which

658 belong to the droplet mode. In this mode, the MSEs of $(NH_4)_2SO_4$ and NH_4NO_3 and
659 OM were higher while those of the other chemical species were lower than the overall
660 particle MSE. Note that the overall particle MSE depends on the mass concentrations
661 and MSEs of individual chemical components. Thus, the seasonal average MSEs of
662 fine particle were dominated by the seasonal average mass fractions and associated
663 MSEs of $(NH_4)_2SO_4$ and NH_4NO_3 and OM in the droplet mode.
664
665 *Insert Figure 8*
666
667 The sum of the products of seasonal average mass concentration and MSEs of the
668 above three chemical species in the droplet mode was 1.8, 2.1, 2.3 and 2.5 $m^2\ g^{-1}$ in
669 spring, summer, autumn and winter, respectively. As expected, the seasonal variations
670 of fine particle MSE followed the sequences of winter ($3.9\pm0.2\ m^2\ g^{-1}$) > autumn
671 ($3.8\pm0.2\ m^2\ g^{-1}$) > summer ($3.6\pm0.2\ m^2\ g^{-1}$) > spring ($3.5\pm0.1\ m^2\ g^{-1}$). Noticeably, fine
672 particle MSE was determined by the average MSEs of the dominant chemical species,
673 rather than their mass fractions which were much smaller than 1.0.
674 Different from the approach used for fine particle MSE, the MSEs of $(NH_4)_2SO_4$,
675 NH_4NO_3 and OM in the droplet mode were determined using measurement-based their
676 mass size distributions prescribed as log-normal size distributions. In theory (section
677 2.4), the log-normal size distribution of chemical species is determined by three
678 parameters include mass concentration (in the range of 0.43 - 2.1 μm), MMAD and
679 standard deviation (σ), which control the area, mode and scale of the log-normal size

distribution, respectively. Thus, the MSEs of $(NH_4)_2SO_4$, NH_4NO_3 and OM should depend on their MMADs and σ values. Seasonal average σ values of $(NH_4)_2SO_4$, NH_4NO_3 and OM were in the range of 0.18-0.21, 0.18-0.21 and 0.22-0.26, respectively, while the corresponding MMADs in the range of 0.72-0.92, 0.75-0.90 and 0.73-0.78 μm, respectively (Fig. 9). Generally, the seasonal average MSEs of $(NH_4)_2SO_4$, NH_4NO_3 and OM in the droplet mode were higher with the lower σ values (or MMADs) when MMADs (σ values) were close. However, the MSE of OM in summer was 5.2 m^2 g^{-1}, which was lower than 5.3 m^2 g^{-1} in autumn, although σ values and MMADs in summer were lower than those in autumn. This was mainly related with the evident fluctuation the MSE of OM in the range of 0.6-0.7 μm.

Insert Figure 9

In conclusion, the fine particle MSE was determined by the sum of the products of average mass fractions and MSEs of $(NH_4)_2SO_4$ and NH_4NO_3 and OM in the droplet mode. The MSEs of the above three chemical species in the droplet mode depended on both their σ value and MMADs. Generally, fine particle MSE mainly related with OM due to its high mass and MSE in the droplet mode in urban Guangzhou.

4. Summary and implication

Size- and chemically-resolved particle number and mass concentration were measured in urban Guangzhou in different seasons during 2015-2016 and the data were used to estimate particle MSE. SO_4^{2-} and NH_4^+ mainly distributed in the droplet mode,

EC in both condensation and droplet modes, and particle mass, NO_3^-, OC, Na^+, Ca^{2+} and Cl^- in both droplet and coarse modes. The estimated b_{sp} can represent 85-89% of the measured b_{sp} based on the size-segregated chemical compositions according to ISORROPIA II thermodynamic equilibrium model and Mie theory model. The largest contributors to b_{sp} were the chemical species in the droplet mode with the highest MSEs.

MSEs of the dominant chemical species were noticeably different in this study than those in the original and revised IMPROVE formulas. The MSEs of $(NH_4)_2SO_4$, NH_4NO_3 and OM in the fine mode were higher than those in the original IMPROVE formula, and in the droplet mode were lower than those in the revised IMPROVE formula. In any case, b_{sp} would be underestimated in urban Guangzhou using the original or revised IMPROVE formulas because the unidentified chemical species (and associated mass fractions) in the droplet mode accounted for a large fraction of b_{sp} and this portion was not included in these formulas. Moreover, MSEs of chemical species would be overestimated in the original and revised IMPROVE formulas using multiple linear regression model when the unidentified species was ignored. In addition, sea salt was found in the coarse mode in this study, differing from the set up in the IMPROVE formulas which is in the droplet mode. It can be concluded that the estimated b_{sp} in Guangzhou based on the revised IMPROVE formula would have large biases, even though good correlations between estimated and measured b_{sp} was found.

MSEs of fine particles are controlled by the relative mass fractions of the dominant chemical components (e.g., $(NH_4)_2SO_4$, NH_4NO_3 and OM) and associated size distributions (e.g. σ and MMAD). Localized b_{sp} formulas are thus needed for better

estimating particle MSE because particle size distributions of individual chemical species vary significantly in space and time.

Data availability. Data used in this study are available from Jun Tao (taojun@scies.org).

Competing interests. The authors declare that they have no conflict of interest.

Acknowledgments

This study was supported by the National Natural Science Foundation of China (No.41475119, No. 41875160 and 41603119). Original data are available from the corresponding authors.

References

Andreae, M. O., Schmid, O., Yang, H., Chand, D., Zhen Yu, J., Zeng, L. M., and Zhang, Y. H.: Optical properties and chemical composition of the atmospheric aerosol in urban Guangzhou, China, Atmospheric Environment, 42, 6335-6350, 2008.

Bergin, M. H., Ogren, J. A., Schwartz, S. E., and McInnes, L. M.: Evaporation of Ammonium Nitrate Aerosol in a Heated Nephelometer: Implications for Field Measurements, Environmental Science & Technology, 31, 2878-2883, 10.1021/es970089h, 1997.

Bian, Q., Huang, X. H., and Yu, J. Z.: One-year observations of size distribution characteristics of major aerosol constituents at a coastal receptor site in Hong Kong – Part 1: Inorganic ions and oxalate, Atmospheric Chemistry and Physics, 14, 9013-9027, 2014.

Cabada, J. C., Rees, S., Takahama, S., Khlystov, A., Pandis, S. N., Davidson, C. I., and Robinson, A. L.: Mass size distributions and size resolved chemical composition of fine particulate matter at the Pittsburgh supersite, Atmospheric Environment, 38, 3127-3141, 2004.

Cao, J., Wang, Q., Chow, J. C., Watson, J. G., Tie, X., Shen, Z., Wang, P., and An, Z.: Impacts of aerosol compositions on visibility impairment in Xi'an, China, Atmospheric Environment, 59, 559-566, 2012.

Chen, P., Wang, T., Lu, X., Yu, Y., Kasoar, M., Xie, M., and Zhuang, B.: Source apportionment of size-fractionated particles during the 2013 Asian Youth Games and the 2014 Youth Olympic Games in Nanjing, China, Science of The Total Environment, 579, 860-870, 2017.

Cheng, Y., Wiedensohler, A., Eichler, H., Su, H., Gnauk, T., Brüggemann, E., Herrmann, H., Heintzenberg, J., Slanina, J., and Tuch, T.: Aerosol optical properties and related chemical apportionment at Xinken in Pearl River Delta of China, Atmospheric Environment, 42, 6351-6372, 2008.

Cheng, Y. F., Berghof, M., Garland, R. M., Wiedensohler, A., Wehner, B., Muller, T. J., Su, H., Zhang, Y. H., Achtert, P., and Nowak, A.: Influence of soot mixing state on aerosol light absorption and

single scattering albedo during air mass aging at a polluted regional site in northeastern China, Journal of Geophysical Research, 114, 2009.
Cheng, Z., Jiang, J. S., Chen, C., Gao, J., Wang, S., Watson, J. G., Wang, H., Deng, J., Wang, B., and Zhou, M.: Estimation of aerosol mass scattering efficiencies under high mass loading: case study for the megacity of Shanghai, China, Environmental Science & Technology, 49, 831-838, 2015.
Chow, J. C., Watson, J. G., Lowenthal, D. H., Chen, L. W. A., and Motallebi, N.: $PM_{2.5}$ source profiles for black and organic carbon emission inventories, Atmospheric Environment, 45, 5407-5414, 2011.
Day, M. C., Zhang, M., and Pandis, S. N.: Evaluation of the ability of the EC tracer method to estimate secondary organic carbon, Atmospheric Environment, 112, 317-325, 2015.
Dong, Y., Hays, M. D., Smith, N. D., and Kinsey, J. S.: Inverting cascade impactor data for size-resolved characterization of fine particulate source emissions, Journal of Aerosol Science, 35, 1497-1512, 2004.
Fountoukis, C., and Nenes, A.: ISORROPIA II: a computationally efficient thermodynamic equilibrium model for K^+–Ca^{2+}–Mg^{2+}–NH_4^+–Na^+–SO_4^{2-} – NO_3^-–Cl^-–H_2O aerosols, Atmospheric Chemistry and Physics, 7, 4639-4659, 2007.
Gao, Y., Lai, S., Lee, S. C., Yau, P. S., Huang, Y., Cheng, Y., Wang, T., Xu, Z., Yuan, C., and Zhang, Y.: Optical properties of size-resolved particles at a Hong Kong urban site during winter, Atmospheric Research, 155, 1-12, 2015.
Gentner, D. R., Isaacman, G., Worton, D. R., Chan, A. W. H., Dallmann, T. R., Davis, L. E., Liu, S., Day, D. A., Russell, L. M., and Wilson, K. R.: Elucidating secondary organic aerosol from diesel and gasoline vehicles through detailed characterization of organic carbon emissions, Proceedings of the National Academy of Sciences of the United States of America, 109, 18318-18323, 2012.
Gentner, D. R., Jathar, S. H., Gordon, T. D., Bahreini, R., Day, D. A., Haddad, I. E., Hayes, P. L., Pieber, S. M., Platt, S. M., and De Gouw, J. A.: Review of Urban Secondary Organic Aerosol Formation from Gasoline and Diesel Motor Vehicle Emissions, Environmental Science & Technology, 51, 1074-1093, 2017.
Guo, S., Hu, M., Wang, Z., Slanina, J., and Zhao, Y.: Size-resolved aerosol water-soluble ionic compositions in the summer of Beijing: implication of regional secondary formation, Atmospheric Chemistry and Physics, 10, 947-959, 2009.
Hallquist, M., Wenger, J., Baltensperger, U., Rudich, Y., Simpson, D., Claeys, M., Dommen, J., Donahue, N., George, C., and Goldstein, A.: The formation, properties and impact of secondary organic aerosol: current and emerging issues, Atmospheric Chemistry and Physics, 9, 5155-5236, 2009.
Han, T., Liu, X., Zhang, Y., Qu, Y., Gu, J., Ma, Q., Lu, K., Tian, H., Chen, J., and Zeng, L.: Characteristics of aerosol optical properties and their chemical apportionments during CAREBeijing 2006, Aerosol and Air Quality Research, 14, 1431-1442, 2014.
Hand, J., Kreidenweis, S., Sherman, D. E., Collett, J., Hering, S., Day, D., and Malm, W.: Aerosol size distributions and visibility estimates during the Big Bend regional aerosol and visibility observational (BRAVO) study, Atmospheric Environment, 36, 5043-5055, 2002.
Hand, J. L., and Malm, W. C.: Review of the IMPROVE equation for estimating ambient light extinction coefficients, CIRA, Colorado State University, 2007.
He, L.Y., Huang, X.F., Xue, L., Hu, M., Lin, Y., Zheng, J., Zhang, R., and Zhang, Y.H.: Submicron aerosol analysis and organic source apportionment in an urban atmosphere in Pearl River Delta of China using high-resolution aerosol mass spectrometry, Journal of Geophysical Research: Atmospheres, 116, 10.1029/2010JD014566, 2011.

Ho, K., Lee, S., Chow, J. C., and Watson, J. G.: Characterization of PM_{10} and $PM_{2.5}$ source profiles for fugitive dust in Hong Kong, Atmospheric Environment, 37, 1023-1032, 2003.

Hua, Y., Cheng, Z., Wang, S., Jiang, J., Chen, D., Cai, S., Fu, X., Fu, Q., Chen, C., Xu, B., and Yu, J.: Characteristics and source apportionment of $PM_{2.5}$ during a fall heavy haze episode in the Yangtze River Delta of China, Atmospheric Environment, 123, 380-391, https://doi.org/10.1016/j.atmosenv.2015.03.046, 2015.

Huang, K., Zhuang, G., Lin, Y., Fu, J., Wang, Q., Liu, T., Zhang, R., Jiang, Y., Deng, C., and Fu, Q.: Typical types and formation mechanisms of haze in an Eastern Asia megacity, Shanghai, Atmospheric Chemistry and Physics, 12, 2012.

Huang, X., Yu, J. Z., He, L. Y., and Hu, M.: Size Distribution Characteristics of Elemental Carbon Emitted from Chinese Vehicles: Results of a Tunnel Study and Atmospheric Implications, Environmental Science & Technology, 40, 5355-5360, 2006a.

Huang, X. F., Yu, J. Z., He, L. Y., and Yuan, Z.: Water‐soluble organic carbon and oxalate in aerosols at a coastal urban site in China: Size distribution characteristics, sources, and formation mechanisms, Journal of Geophysical Research: Atmospheres, 111, 2006b.

John, W., Wall, S. M., Ondo, J. L., and Winklmayr, W.: Modes in the size distributions of atmospheric inorganic aerosol, Atmospheric Environment, 24, 2349-2359, 1990.

Jung, J., Lee, H., Kim, Y. J., Liu, X., Zhang, Y., Gu, J., and Fan, S.: Aerosol chemistry and the effect of aerosol water content on visibility impairment and radiative forcing in Guangzhou during the 2006 Pearl River Delta campaign, Journal of Environmental Management, 90, 3231-3244, 2009a.

Jung, J., Lee, H., Kim, Y. J., Liu, X., Zhang, Y., Hu, M., and Sugimoto, N.: Optical properties of atmospheric aerosols obtained by in situ and remote measurements during 2006 Campaign of Air Quality Research in Beijing (CAREBeijing‐2006), Journal of Geophysical Research: Atmospheres (1984–2012), 114, 2009b.

Kulkarni, P., Baron, P. A., and Willeke, K.: Aerosol measurement: principles, techniques, and applications, John Wiley & Sons, 2011.

Lan, Z., Chen, D., Li, X., Huang, X., He, L., Deng, Y., Feng, N., and Hu, M.: Modal characteristics of carbonaceous aerosol size distribution in an urban atmosphere of South China, Atmospheric Research, 100, 51-60, 2011.

Li, H., Wang, Q. G., Yang, M., Li, F., Wang, J., Sun, Y., Wang, C., Wu, H., and Qian, X.: Chemical characterization and source apportionment of $PM_{2.5}$ aerosols in a megacity of Southeast China, Atmospheric Research, 181, 288-299, http://doi.org/10.1016/j.atmosres.2016.07.005, 2016.

Lin, C., Li, Y., Yuan, Z., Lau, A. K. H., Li, C., and Fung, J. C. H.: Using satellite remote sensing data to estimate the high-resolution distribution of ground-level $PM_{2.5}$, Remote Sensing of Environment, 156, 117-128, https://doi.org/10.1016/j.rse.2014.09.015, 2015.

Lowenthal, D. H., and Kumar, N.: Variation of Mass Scattering Efficiencies in IMPROVE, Journal of The Air & Waste Management Association, 54, 926-934, 2004.

Malm, W., Sisler, J., Pitchford, M., Scruggs, M., Ames, R., Copeland, S., Gebhart, K., and Day, D.: IMPROVE (interagency monitoring of protected visual environments): spatial and seasonal patterns and temporal variability of haze and its constituents in the United States: Report III, CIRA Report ISSN, 0737-5352, 2000.

Malm, W. C., Sisler, J. F., Huffman, D., Eldred, R. A., and Cahill, T. A.: Spatial and seasonal trends in

particle concentration and optical extinction in the United States, Journal of Geophysical Research, 99, 1347-1370, 1994.

Malm, W. C., and Pitchford, M.: Comparison of calculated sulfate scattering efficiencies as estimated from size-resolved particle measurements at three national locations, Atmospheric Environment, 31, 1315-1325, 1997.

Malm, W. C., Day, D. E., Kreidenweis, S. M., Collett, J. L., and Lee, T.: Humidity-dependent optical properties of fine particles during the Big Bend Regional Aerosol and Visibility Observational Study, Journal of Geophysical Research, 108, 4279, 2003.

Malm, W. C., and Hand, J. L.: An examination of the physical and optical properties of aerosols collected in the IMPROVE program, Atmospheric Environment, 41, 3407-3427, 2007.

Ming, L., Jin, L., Li, J., Fu, P., Yang, W., Liu, D., Zhang, G., Wang, Z., and Li, X.: $PM_{2.5}$ in the Yangtze River Delta, China: Chemical compositions, seasonal variations, and regional pollution events, Environmental Pollution, 223, 200-212, https://doi.org/10.1016/j.envpol.2017.01.013, 2017.

Pitchford, M., Malm, W., Schichtel, B., Kumar, N., Lowenthal, D., and Hand, J.: Revised algorithm for estimating light extinction from IMPROVE particle speciation data, Journal of the Air & Waste Management Association, 57, 1326-1336, 2007.

Schwarz, J., Gao, R., Spackman, J., Watts, L., Thomson, D., Fahey, D., Ryerson, T., Peischl, J., Holloway, J., and Trainer, M.: Measurement of the mixing state, mass, and optical size of individual black carbon particles in urban and biomass burning emissions, Geophysical Research Letters, 35, 2008.

Shen, G., Xue, M., Yuan, S., Zhang, J., Zhao, Q., Li, B., Wu, H., and Ding, A.: Chemical compositions and reconstructed light extinction coefficients of particulate matter in a mega-city in the western Yangtze River Delta, China, Atmospheric Environment, 83, 14-20, http://dx.doi.org/10.1016/j.atmosenv.2013.10.055, 2014.

Shiraiwa, M., Kondo, Y., Moteki, N., Takegawa, N., Miyazaki, Y., and Blake, D. R.: Evolution of mixing state of black carbon in polluted air from Tokyo, Geophysical Research Letters, 34, 2007.

Sisler, J. F., and Latimer, D. A.: Spatial and temporal patterns and the chemical composition of the haze in the United States: An analysis of data from the IMPROVE network, 1988-1991, Cooperative Institute for Research in the Atmosphere, Colorado State University, 1993.

Sisler, J. F., Malm, W., Gebhart, K., and Pitchford, M. L.: Spatial and Seasonal Patterns and Long Term Variability of the composition of the Haze in the United States, Report ISSN, 0737-5352, 1996.

Sisler, J. F., and Malm, W. C.: Interpretation of Trends of PM25 and Reconstructed Visibility from the IMPROVE Network, Journal of the Air & Waste Management Association, 50, 775-789, 2000.

Sun, J., Shen, Z., Zhang, L., Lei, Y., Gong, X., Zhang, Q., Zhang, T., Xu, H., Cui, S., Wang, Q., Cao, J., Tao, J., Zhang, N., and Zhang, R.: Chemical source profiles of urban fugitive dust PM2.5 samples from 21 cities across China, Science of The Total Environment, 649, 1045-1053, https://doi.org/10.1016/j.scitotenv.2018.08.374, 2019.

Takemura, T., Nakajima, T., Dubovik, O., Holben, B. N., and Kinne, S.: Single-Scattering Albedo and Radiative Forcing of Various Aerosol Species with a Global Three-Dimensional Model, Journal of Climate, 15, 333-352, 2002.

Tao, J., Ho, K., Chen, L., Zhu, L., Han, J., and Xu, Z.: Effect of chemical composition of $PM_{2.5}$ on visibility in Guangzhou, China, 2007 spring, Particuology, 7, 68-75, 2009.

Tao, J., Cao, J.J., Zhang, R.J., Zhu, L., Zhang, T., Shi, S., and Chan, C.Y.: Reconstructed light extinction coefficients using chemical compositions of $PM_{2.5}$ in winter in Urban Guangzhou, China, Advances in Atmospheric Sciences, 29, 359-368, 2012.

888 Tao, J., Zhang, L., Ho, K., Zhang, R., Lin, Z., Zhang, Z., Lin, M., Cao, J., Liu, S., and Wang, G.: Impact
889 of $PM_{2.5}$ chemical compositions on aerosol light scattering in Guangzhou - the largest megacity in
890 South China, Atmospheric Research, 135–136, 48-58,
891 http://dx.doi.org/10.1016/j.atmosres.2013.08.015, 2014.
892 Tao, J., Zhang, L., Cao, J., and Zhang, R.: A review of current knowledge concerning $PM_{2.5}$ chemical
893 composition, aerosol optical properties and their relationships across China, Atmospheric
894 Chemistry and Physics, 17, 9485-9518, 10.5194/acp-17-9485-2017, 2017a.
895 Tao, J., Zhang, L., Cao, J., Zhong, L., Chen, D., Yang, Y., Chen, D., Chen, L., Zhang, Z., Wu, Y., Xia, Y.,
896 Ye, S., and Zhang, R.: Source apportionment of $PM_{2.5}$ at urban and suburban areas of the Pearl River
897 Delta region, south China - With emphasis on ship emissions, Science of The Total Environment,
898 574, 1559-1570, http://dx.doi.org/10.1016/j.scitotenv.2016.08.175, 2017b.
899 Tao, J., Zhang, Z., Tan, H., Zhang, L., Wu, Y., Sun, J., Che, H., Cao, J., Cheng, P., Chen, L., and Zhang,
900 R.: Observational evidence of cloud processes contributing to daytime elevated nitrate in an urban
901 atmosphere, Atmospheric Environment, 186, 209-215,
902 https://doi.org/10.1016/j.atmosenv.2018.05.040, 2018.
903 Tian, S., Pan, Y., Liu, Z., Wen, T., and Wang, Y.: Size-resolved aerosol chemical analysis of extreme haze
904 pollution events during early 2013 in urban Beijing, China, Journal of hazardous materials, 279,
905 452-460, 2014.
906 Titos, G., Foyo-Moreno, I., Lyamani, H., Querol, X., Alastuey, A., and Alados-Arboledas, L.:
907 Optical properties and chemical composition of aerosol particles at an urban location: An
908 estimation of the aerosol mass scattering and absorption efficiencies, Journal of Geophysical
909 Research: Atmospheres, 117, 10.1029/2011JD016671, 2012.
910 Vaughan, N. P.: The Andersen impactor: Calibration, wall losses and numerical simulation, Journal of
911 Aerosol Science, 20, 67-90, 1989.
912 Wang, H., Shi, G., Tian, M., Zhang, L., Chen, Y., Yang, F., and Cao, X.: Aerosol optical properties and
913 chemical composition apportionment in Sichuan Basin, China, Science of The Total Environment,
914 577, 245-257, http://dx.doi.org/10.1016/j.scitotenv.2016.10.173, 2017.
915 Wang, Y., Yao, L., Wang, L., Liu, Z., Ji, D., Tang, G., Zhang, J., Sun, Y., Hu, B., and Xin, J.: Mechanism
916 for the formation of the January 2013 heavy haze pollution episode over central and eastern China,
917 Science China Earth Sciences, 57, 14-25, 2014.
918 Watson, J. G., Chow, J. C., and Houck, J. E.: $PM_{2.5}$ chemical source profiles for vehicle exhaust,
919 vegetative burning, geological material, and coal burning in Northwestern Colorado during 1995,
920 Chemosphere, 43, 1141-1151, 2001.
921 Watson, J. G.: Visibility: Science and regulation, Journal of the Air & Waste Management Association,
922 52, 628-713, 2002.
923 Watson, J. G., Chow, J. C., Lowenthal, D. H., and Magliano, K. L.: Estimating aerosol light scattering at
924 the Fresno Supersite, Atmospheric Environment, 42, 1186-1196, 2008.
925 Wu, C., and Yu, J. Z.: Determination of primary combustion source organic carbon-to-elemental carbon
926 (OC/EC) ratio using ambient OC and EC measurements: Secondary OC-EC correlation
927 minimization method, Atmospheric Chemistry and Physics, 16, 5453-5465, 2016.
928 Wu, Y., Zhang, R., Tian, P., Tao, J., Hsu, S.C., Yan, P., Wang, Q., Cao, J., Zhang, X., and Xia, X.: Effect
929 of ambient humidity on the light absorption amplification of black carbon in Beijing during January

2013, Atmospheric Environment, 124, 217-223, 2016.
Wu, Y., Wang, X., Tao, J., Huang, R., Tian, P., Cao, J., Zhang, L., Ho, K. F., Han, Z., and Zhang, R.: Size distribution and source of black carbon aerosol in urban Beijing during winter haze episodes, Atmospheric Chemistry and Physics, 17, 7965-7975, 10.5194/acp-17-7965-2017, 2017.
Xia, Y., Tao, J., Zhang, L., Zhang, R., Li, S., Wu, Y., Cao, J., Wang, X., Ma, Q., and Xiong, Z.: Impact of size distributions of major chemical components in fine particles on light extinction in urban Guangzhou, Science of The Total Environment, 587-588, 240-247, https://doi.org/10.1016/j.scitotenv.2017.02.127, 2017.
Yao, X., Lau, A. P. S., Fang, M., Chan, C. K., and Hu, M.: Size distributions and formation of ionic species in atmospheric particulate pollutants in Beijing, China: 1-inorganic ions, Atmospheric Environment, 37, 2991-3000, 2003.
Yu, H., Wu, C., Wu, D., and Yu, J.: Size distributions of elemental carbon and its contribution to light extinction in urban and rural locations in the pearl river delta region, China, Atmospheric Chemistry and Physics, 10, 5107-5119, 2010.
Zhang, F., Xu, L., Chen, J., Yu, Y., Niu, Z., and Yin, L.: Chemical compositions and extinction coefficients of $PM_{2.5}$ in peri-urban of Xiamen, China, during June 2009–May 2010, Atmospheric Research, 106, 150-158, 2012a.
Zhang, H., Wang, S., Hao, J., Wan, L., Jiang, J. S., Zhang, M., Mestl, H. E. S., Alnes, L. W. H., Aunan, K., and Mellouki, A. W.: Chemical and size characterization of particles emitted from the burning of coal and wood in rural households in Guizhou, China, Atmospheric Environment, 51, 94-99, 2012b.
Zhang, L., Vet, R., Wiebe, A., Mihele, C., Sukloff, B., Chan, E., Moran, M. D., and Iqbal, S.: Characterization of the size-segregated water-soluble inorganic ions at eight Canadian rural sites, Atmospheric Chemistry and Physics, 8, 7133-7151, 2008.
Zhang, R., Jing, J., Tao, J., Hsu, S. C., Wang, G., Cao, J., Lee, C. S. L., Zhu, L., Chen, Z., Zhao, Y., and Shen, Z.: Chemical characterization and source apportionment of $PM_{2.5}$ in Beijing: seasonal perspective, Atmos. Chem. Phys., 13, 7053-7074, 10.5194/acp-13-7053-2013, 2013.
Zhang, R., Wang, G., Guo, S., Zamora, M. L., Ying, Q., Lin, Y., Wang, W., Hu, M., and Wang, Y.: Formation of urban fine particulate matter, Chemical reviews, 115, 3803-3855, 2015a.
Zhang, Z., Engling, G., Zhang, L., Kawamura, K., Yang, Y., Tao, J., Zhang, R., Chan, C., and Li, Y.: Significant influence of fungi on coarse carbonaceous and potassium aerosols in a tropical rainforest, Environmental Research Letters, 10, 034015, 2015b.
Zhang, Z., Gao, J., Engling, G., Tao, J., Chai, F., Zhang, L., Zhang, R., Sang, X., Chan, C.Y., and Lin, Z.: Characteristics and applications of size-segregated biomass burning tracers in China's Pearl River Delta region, Atmospheric Environment, 102, 290-301, 2015c.
Zhao, X. J., Zhao, P. S., Xu, J., Meng, W., Pu, W., Dong, F., He, D., and Shi, Q. F.: Analysis of a winter regional haze event and its formation mechanism in the North China Plain, Atmospheric Chemistry and Physics, 13, 5685-5696, 2013.
Zheng, B., Tong, D., Li, M., Liu, F., Hong, C., Geng, G., Li, H., Li, X., Peng, L., Qi, J., Yan, L., Zhang, Y., Zhao, H., Zheng, Y., He, K., and Zhang, Q.: Trends in China's anthropogenic emissions since 2010 as the consequence of clean air actions, Atmospheric Chemistry and Physics, 18, 14095-14111, 10.5194/acp-18-14095-2018, 2018.
Zheng, J., Zhang, L., Che, W., Zheng, Z., and Yin, S.: A highly resolved temporal and spatial air pollutant emission inventory for the Pearl River Delta region, China and its uncertainty assessment,

974 Atmospheric Environment, 43, 5112-5122, 2009.
975 Zheng, M., Hagler, G. S. W., Ke, L., Bergin, M. H., Wang, F., Louie, P. K. K., Salmon, L. G., Sin, D. W.
976 M., Yu, J. Z., and Schauer, J. J.: Composition and sources of carbonaceous aerosols at three
977 contrasting sites in Hong Kong, Journal of Geophysical Research, 111, 2006.
978 Zhuang, H., Chan, C. K., Fang, M., and Wexler, A. S.: Formation of nitrate and non-sea-salt sulfate on
979 coarse particles, Atmospheric Environment, 33, 4223-4233, 1999a.
980 Zhuang, H., Chan, C. K., Fang, M., and Wexler, A. S.: Size distributions of particulate sulfate, nitrate,
981 and ammonium at a coastal site in Hong Kong, Atmospheric Environment, 33, 843-853, 1999b.
982 Zou, J., Liu, Z., Hu, B., Huang, X., Wen, T., Ji, D., Liu, J., Yang, Y., Yao, Q., and Wang, Y.: Aerosol
983 chemical compositions in the North China Plain and the impact on the visibility in Beijing and
984 Tianjin, Atmospheric Research, 201, 235-246, https://doi.org/10.1016/j.atmosres.2017.09.014,
985 2018.

Table 1. Summary of the sampling information

Season	Date	Sample type	Instruments	Sample duration	Sample number
Summer	15 July- 6 August in 2015	Size-segregated samples	Anderson 8-stage air samplers	24h	23 sets
Autumn	15 October- 5 November in 2015			24h	22 sets
Winter	4-20 January - 19-22 February in 2016			24h	21 sets
Spring	8-20 April and 4-14 May in 2016			48h	10 sets
Summer	15 July- 6 August in 2015	$PM_{2.5}$ and PM_{10} samples	GSAPM	24 h	23 sets
Autumn	15 October- 5 November in 2015				22 sets
Winter	4-20 January - 19-22 February in 2016				21 sets
Spring	8-20 April and 4-14 May in 2016				20 sets
Summer	15 July- 6 August in 2015	Particle number concentration in the range of 14 nm - 615 nm	SMPS, TSI Model 3936	5 min	
Autumn	15 October- 5 November in 2015				
Winter	4-20 January - 19-22 February in 2016				
Spring	8-20 April and 4-14 May in 2016				
Summer	15 July- 6 August in 2015	Particle number concentration in the range of 542 nm - 10 µm	APS, TSI Model 3321	5 min	
Autumn	15 October- 5 November in 2015				
Winter	4-20 January - 19-22 February in 2016				
Spring	8-20 April and 4-14 May in 2016				
Summer	15 July- 6 August in 2015	Dry b_{sp}	Nephelometer, Ecotech, Model Aurora1000G	5 min	
Autumn	15 October- 5 November in 2015				
Winter	4-20 January - 19-22 February in 2016				
Spring	8-20 April and 4-14 May in 2016				
Summer	15 July- 6 August in 2015	NO_3^- in PM_{10}	IGAC, Model S-611	1 h	
Autumn	15 October- 5 November in 2015	NO_3^- in $PM_{2.5}$			
Winter	4-20 January in 2016	NO_3^- in $PM_{2.5}$			
Spring	4-14 May in 2016	NO_3^- in $PM_{2.5}$			

Table 2. Summary of concentrations of chemical compositions in the different size modes

Chemical composition	Size mode	Annual		Spring		Summer		Autumn		Winter	
		MMAD[b] (μm)	Mass (μg m^{-3})	MMAD (μm)	Mass (μg m^{-3})	MMAD (μm)	Mass (μg m^{-3})	MMAD (μm)	Mass (μg m^{-3})	MMAD (μm)	Mass (μg m^{-3})
PM[a]	Condensation(<0.43μm)	—	5.7±2.3 (10±2%)	—	6.6±3.0 (10±3%)	—	4.0±1.3 (8±1%)	—	7.0±1.9 (10±2%)	0.21±0.00	5.7±2.2 (10±2%)
	Droplet(0.43 -2.1μm)	0.78±0.07	29.1±11.8(48±7%)	0.87±0.13	31.9±8.7(50±8%)	0.78±0.05	20.4±8.0(42±8%)	0.74±0.06	35.6±9.7(46±4%)	0.79±0.05	30.6±13.2(52±5%)
	Coarse(2.1 -10μm)	4.57±0.42	25.5±10.1(42±8%)	4.37±0.37	25.3±7.0(40±7%)	4.47±0.35	23.1±4.9(50±7%)	4.90±0.46	30.8±11.8(44±6%)	4.47±0.24	22.5±11.7(38±6%)
SO_4^{2-}	Condensation(<0.43μm)	—	1.0±0.5 (12%)	—	0.9±0.3 (10%)	—	0.9±0.3 (15%)	—	1.4±0.5 (13%)	0.21±0.00	0.6±0.3 (10%)
	Droplet(0.43 -2.1μm)	0.80±0.08	6.5±2.9 (77%)	0.86±0.07	7.3±2.3 (79%)	0.79±0.07	4.9±2.6 (75%)	0.77±0.08	8.5±2.6 (75%)	0.82±0.08	5.8±2.7 (79%)
	Coarse(2.1 -10μm)	4.17±0.44	0.9±0.6 (11%)	4.34±0.59	0.9±0.6 (11%)	4.09±0.16	0.6±0.3 (10%)	4.08±0.22	1.4±0.8 (12%)	4.20±0.59	0.8±0.5 (11%)
NO_3^-	Condensation(<0.43μm)	—	0.4±0.3 (10%)	—	0.4±0.2 (6%)	—	0.2±0.2 (9%)	—	0.4±0.3 (10%)	0.21±0.00	0.6±0.3 (13%)
	Droplet(0.43 -2.1μm)	0.85±0.21	2.2±2.2 (46%)	0.87±0.07	3.2±2.1 (51%)	0.94±0.35	0.8±0.5 (35%)	0.80±0.09	2.1±1.7 (39%)	0.80±0.07	3.2±2.9 (63%)
	Coarse(2.1 -10μm)	4.38±0.61	1.8±1.4 (44%)	4.47±0.62	2.4±1.2 (43%)	4.15±0.52	1.3±0.7 (56%)	4.36±0.31	2.4±1.7 (51%)	4.74±0.76	1.3±1.5 (24%)
NH_4^+	Condensation(<0.43μm)	—	0.2±0.2 (6%)	—	0.2±0.1 (6%)	—	0.1±0.1 (5%)	—	0.2±0.2 (7%)	0.21±0.00	0.2±0.2 (6%)
	Droplet(0.43 -2.1μm)	0.76±0.13	2.4±1.5 (89%)	0.86±0.17	2.8±1.1 (89%)	0.70±0.11	1.4±1.1 (91%)	0.73±0.12	3.1±1.4 (90%)	0.82±0.10	2.5±1.7 (86%)
	Coarse(2.1 -10μm)	3.25±0.69	0.1±0.1 (5%)	3.13±1.16	0.2±0.2 (6%)	3.36±0.68	0.0±0.0 (4%)	3.01±0.23	0.1±0.1 (3%)	3.45±0.70	0.2±0.1 (8%)
OC	Condensation(<0.43μm)	0.21±0.00	1.2±0.6 (13±4%)	—	1.4±0.4 (19±4%)	—	0.8±0.3 (11±4%)	—	1.6±0.5 (14±2%)	0.21±0.00	1.2±0.6 (13±4%)
	Droplet(0.43 -2.1μm)	0.76±0.07	5.5±2.4 (62±9%)	0.73±0.06	3.9±1.6 (51±6%)	0.77±0.07	4.1±1.3 (63±9%)	0.78±0.06	6.9±2.0 (58±5%)	0.75±0.08	6.5±2.6 (69±7%)
	Coarse(2.1 -10μm)	3.73±0.58	2.2±1.1 (25±8%)	3.99±0.25	2.2±0.7 (30±3%)	3.50±0.73	1.7±0.9 (26±9%)	4.14±0.24	3.3±1.0 (28±4%)	3.44±0.39	1.7±0.9 (18±8%)
EC	Condensation(<0.43μm)	—	1.1±0.4 (31±7%)	—	1.1±0.1 (36±9%)	0.21±0.00	0.8±0.2 (32±5%)	—	1.0±0.4 (24±3%)	0.21±0.00	1.4±0.6 (35±6%)
	Droplet(0.43 -2.1μm)	0.66±0.08	2.0±1.0 (55±7%)	0.65±0.08	1.8±0.8 (54±9%)	0.61±0.08	1.3±0.5 (50±5%)	0.71±0.04	2.7±0.9 (62±6%)	0.67±0.07	2.1±0.9 (54±5%)
	Coarse(2.1 -10μm)	3.69±0.65	0.5±0.3 (14±7%)	3.54±0.61	0.3±0.2 (10±6%)	3.48±0.52	0.5±0.3 (18±6%)	4.17±0.24	0.6±0.2 (14±5%)	3.50±0.75	0.4±0.3 (11±8%)
Na^+	Condensation(<0.43μm)	—	0.1±0.1 (11%)	—	0.1±0.0 (9%)	—	0.0±0.0 (5%)	—	0.1±0.1 (16%)	0.21±0.00	0.1±0.0 (11%)
	Droplet(0.43 -2.1μm)	0.86±0.12	0.4±0.2 (48%)	0.84±0.10	0.3±0.0 (48%)	0.96±0.11	0.4±0.1 (45%)	0.81±0.09	0.4±0.3 (52%)	0.80±0.11	0.3±0.2 (48%)
	Coarse(2.1 -10μm)	3.75±0.38	0.4±0.3 (41%)	3.90±0.63	0.3±0.2 (43%)	3.60±0.19	0.6±0.4 (50%)	3.64±0.27	0.3±0.3 (32%)	3.94±0.38	0.3±0.2 (41%)
K^+	Condensation(<0.43μm)	—	0.1±0.0 (13%)	—	0.0±0.0 (10%)	—	0.1±0.0 (16%)	—	0.1±0.0 (12%)	0.21±0.00	0.1±0.0 (12%)
	Droplet(0.43 -2.1μm)	0.69±0.08	0.3±0.2 (78%)	0.76±0.07	0.3±0.1 (76%)	0.64±0.08	0.3±0.1 (72%)	0.67±0.07	0.4±0.2 (87%)	0.73±0.06	0.4±0.2 (77%)
	Coarse(2.1 -10μm)	3.74±0.51	0.0±0.0 (9%)	3.94±0.40	0.1±0.0 (14%)	3.74±0.64	0.0±0.0 (12%)	3.30±0.38	0.0±0.0 (1%)	3.78±0.35	0.0±0.0 (11%)
Ca^{2+}	Condensation(<0.43μm)	—	0.0±0.0 (4%)	—	0.1±0.0 (7%)	—	0.0±0.0 (4%)	—	0.0±0.0 (3%)	0.21±0.00	0.0±0.0 (5%)
	Droplet(0.43 -2.1μm)	0.91±0.12	0.2±0.1 (24%)	0.88±0.13	0.3±0.1 (36%)	1.00±0.11	0.3±0.1 (30%)	0.81±0.10	0.2±0.1 (16%)	0.92±0.09	0.2±0.1 (21%)
	Coarse(2.1 -10μm)	4.57±0.54	0.8±0.4 (72%)	5.02±0.58	0.6±0.2 (57%)	4.10±0.42	0.7±0.3 (66%)	4.72±0.47	1.1±0.5 (81%)	4.73±0.38	0.7±0.3 (74%)
Cl^-	Condensation(<0.43μm)	—	0.0±0.0 (5%)	—	0.1±0.0 (5%)	—	0.0±0.0 (2%)	—	0.0±0.0 (5%)	0.21±0.00	0.0±0.0 (10%)
	Droplet(0.43 -2.1μm)	0.89±0.13	0.2±0.3 (24%)	0.89±0.10	0.7±0.7 (37%)	0.92±0.20	0.0±0.0 (9%)	0.89±0.05	0.0±0.0 (17%)	0.85±0.08	0.2±0.2 (42%)
	Coarse(2.1 -10μm)	3.77±0.35	0.4±0.4 (71%)	3.97±0.12	0.8±0.4 (58%)	3.70±0.23	0.4±0.3 (89%)	3.72±0.21	0.3±0.2 (78%)	3.80±0.50	0.4±0.6 (48%)

[a]PM: Particulate matter; [b] MMAD is mass mean aerodynamic diameter.

Table 3. Summary of the estimated MSEs of particle and the dominant chemical composition at the wavelength of 550nm under dry condition (relative humidity =40%)

Chemical species	Size mode	Annual		Spring		Summer		Autumn		Winter	
		MMAD[c] (μm)	MSE[d] (m^2 g^{-1})	MMAD (μm)	MSE (m^2 g^{-1})	MMAD (μm)	MSE (m^2 g^{-1})	MMAD (μm)	MSE (m^2 g^{-1})	MMAD (μm)	MSE (m^2 g^{-1})
PM[a]	Condensation(<0.43μm)	—	2.1±0.2	—	1.9±0.2	—	2.0±0.1	—	2.1±0.1	0.21±0.00	2.2±0.2
	Droplet(0.43 -2.1μm)	0.78±0.07	4.3±0.2	0.87±0.13	4.0±0.1	0.78±0.05	4.2±0.1	0.74±0.06	4.3±0.2	0.79±0.05	4.4±0.2
	Coarse(2.1 -10μm)	4.57±0.42	0.5±0.0	4.37±0.37	0.6±0.1	4.47±0.35	0.5±0.0	4.90±0.46	0.5±0.0	4.47±0.24	0.5±0.0
	Fine mode(<2.1μm)[b]		3.7±0.2		3.5±0.1		3.6±0.2		3.8±0.2		3.9±0.2
$(NH_4)_2SO_4$	Condensation(<0.43μm)	—	2.1±0.5	—	1.9±0.6	—	2.6±0.2	—	2.0±0.5	0.21±0.00	1.9±0.5
	Droplet(0.43 -2.1μm)	0.79±0.17	4.7±0.6	0.92±0.13	4.3±0.3	0.74±0.20	4.8±0.6	0.72±0.16	4.9±0.7	0.84±0.13	4.6±0.7
	Fine mode(<2.1μm)		4.4±0.8		4.1±0.4		4.5±0.6		4.6±0.8		4.3±0.9
NH_4NO_3	Condensation(<0.43μm)	0.21±0.00	2.3±0.8	—	2.0±0.8	—	2.9±0.3	—	2.6±1.0	0.21±0.00	2.3±0.7
	Droplet(0.43 -2.1μm)	0.80±0.16	4.8±0.9	0.90±0.18	4.5±0.8	0.77±0.17	4.9±0.8	0.75±0.13	5.1±1.0	0.82±0.14	4.7±0.8
	Fine mode(<2.1μm)		4.5±1.5		4.2±1.2		4.7±0.9		4.9±2.0		4.4±1.3
OM	Condensation(<0.43μm)	—	2.7±0.1	—	2.5±0.1	—	2.8±0.2	—	2.6±0.1	0.21±0.00	2.8±0.1
	Droplet(0.43 -2.1μm)	0.76±0.07	5.3±0.2	0.73±0.06	5.4±0.1	0.77±0.07	5.2±0.2	0.78±0.06	5.3±0.2	0.75±0.08	5.5±0.2
	Coarse(2.1 -10μm)	3.73±0.58	0.8±0.1	3.99±0.25	0.8±0.0	3.50±0.73	0.8±0.1	4.14±0.24	0.7±0.0	3.44±0.39	0.8±0.1
	Fine mode(<2.1μm)		4.6±0.3		4.4±0.2		4.6±0.2		4.5±0.1		4.9±0.3
EC	Condensation(<0.43μm)	—	2.9±0.1	—	2.9±0.1	—	2.9±0.1	—	3.0±0.1	0.21±0.00	2.9±0.1
	Droplet(0.43 -2.1μm)	0.66±0.08	2.3±0.2	0.65±0.08	2.3±0.2	0.61±0.08	2.3±0.2	0.71±0.04	2.2±0.1	0.67±0.07	2.3±0.2
	Coarse(2.1 -10μm)	3.69±0.65	0.4±0.0	3.54±0.61	0.4±0.0	3.48±0.52	0.4±0.0	4.17±0.24	0.4±0.0	3.50±0.75	0.5±0.0
	Fine mode(<2.1μm)		2.6±0.1		2.6±0.1		2.6±0.2		2.5±0.1		2.6±0.1
Crustal element oxides	Condensation(<0.43μm)	—	0.7±0.0	—	0.7±0.0	—	0.7±0.1	—	0.7±0.0	0.21±0.00	0.7±0.0
	Droplet(0.43 -2.1μm)	0.91±0.12	2.9±0.2	0.88±0.13	3.0±0.2	1.00±0.11	2.9±0.2	0.81±0.10	2.8±0.2	0.92±0.09	2.8±0.2
	Coarse(2.1 -10μm)	4.57±0.54	0.4±0.0	5.02±0.58	0.4±0.0	4.10±0.42	0.5±0.0	4.72±0.47	0.4±0.0	4.73±0.38	0.4±0.0
	Fine mode(<2.1μm)		2.4±0.2		2.4±0.1		2.5±0.2		2.4±0.2		2.3±0.2
Unidentified	Condensation(<0.43μm)	—	1.3±0.2	—	1.2±0.4	—	1.2±0.2	—	1.4±0.1	0.21±0.00	1.3±0.2
	Droplet(0.43 -2.1μm)	0.85±0.26	3.8±0.6	1.00±0.20	3.5±0.8	0.74±0.44	3.9±0.9	0.84±0.10	3.9±0.2	0.90±0.20	3.7±0.4
	Coarse(2.1 -10μm)	5.74±1.52	0.4±0.1	4.55±0.71	0.5±0.1	6.46±1.14	0.4±0.1	6.33±1.62	0.4±0.1	4.91±0.90	0.5±0.1
	Fine mode(<2.1μm)		3.1±0.8		2.9±0.9		2.6±1.0		3.3±0.3		3.1±0.5
NaCl	Coarse(2.1 -10μm)	4.88±0.41	0.5±0.1	5.14±0.70	0.5±0.1	4.49±0.38	0.6±0.0	5.38±0.43	0.5±0.0	4.66±0.65	0.5±0.0

[a]PM: Particulate matter; [b]Fine mode = sum of condensation and droplet modes; [c]MMAD is mass mean aerodynamic diameter; [d]MSE is mass scattering efficiency.

List of Figures

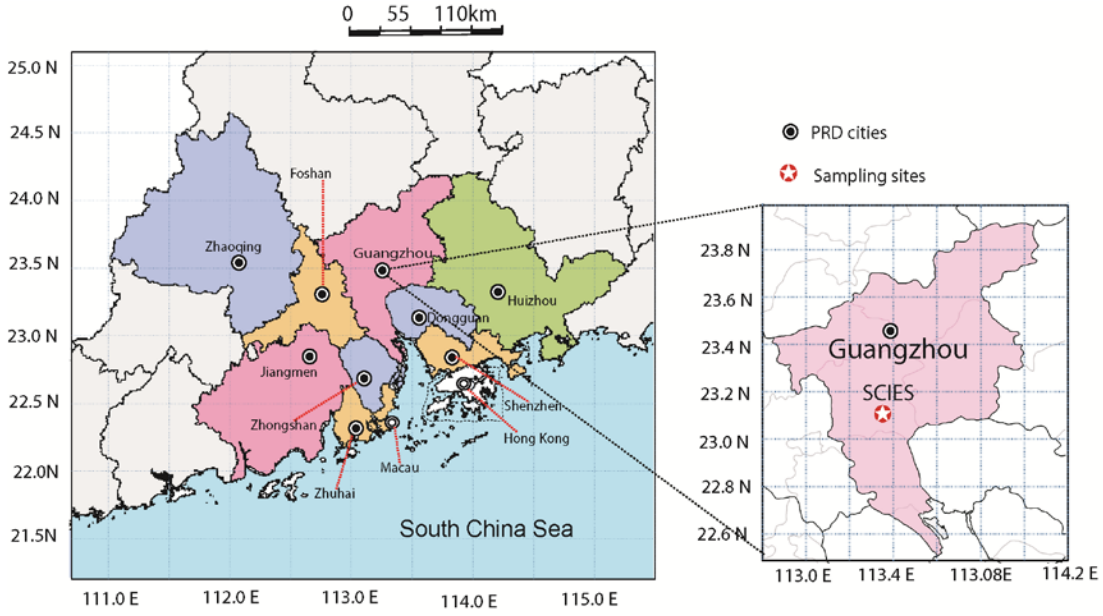

Fig. 1. The sampling location in urban Guangzhou in the Pearl River Delta (PRD) region of China.

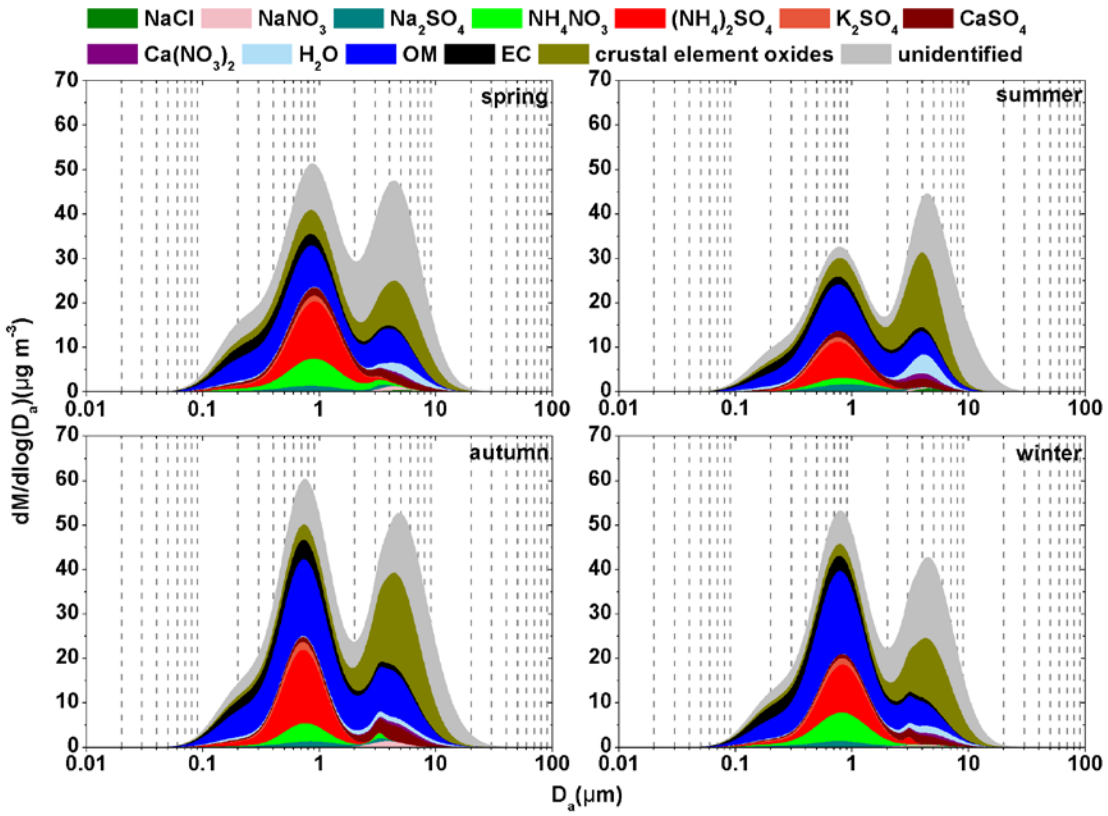

Fig. 2. Continuous log-normal size distributions of chemical species mass concentrations in four seasons ($dlogD_a$=0.01μm).

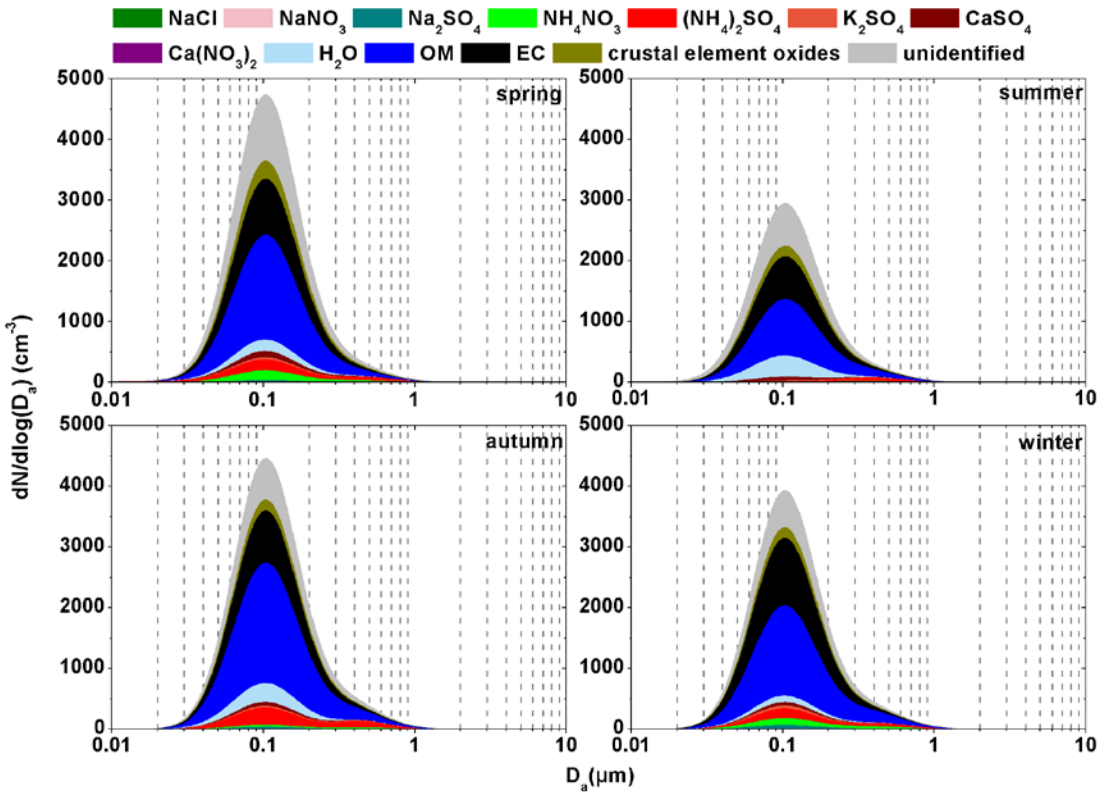

Fig. 3. Continuous log-normal size distributions of the estimated chemical species number concentrations in four seasons ($dlogD_a$=0.01μm).

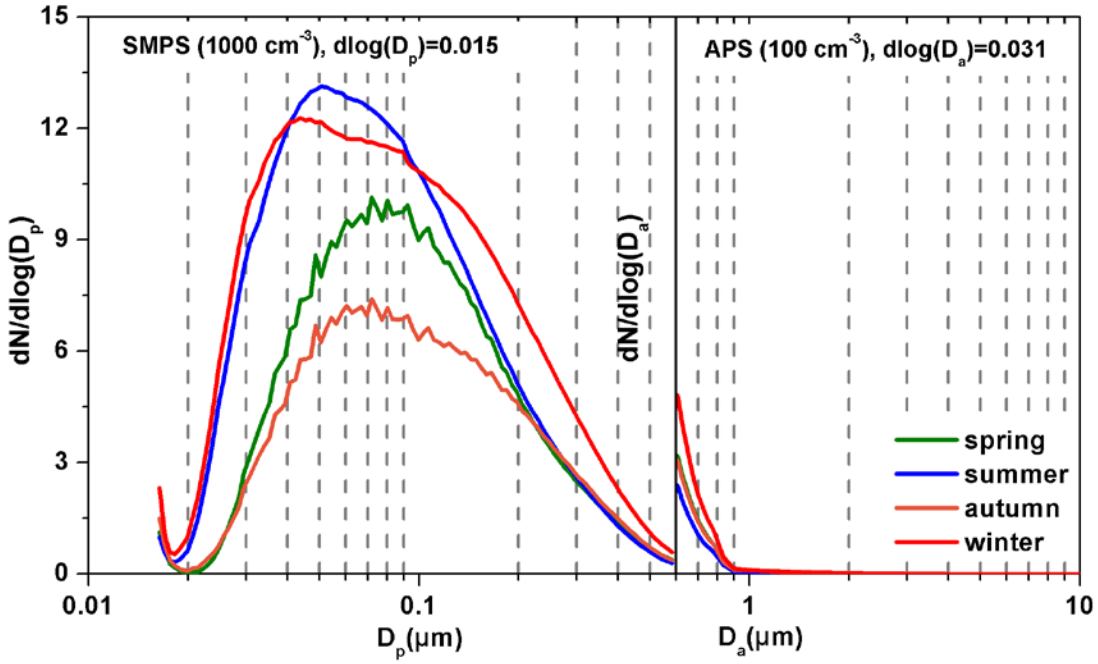

Fig. 4. Continuous log-normal size distributions of the measured particle number concentrations in four seasons.

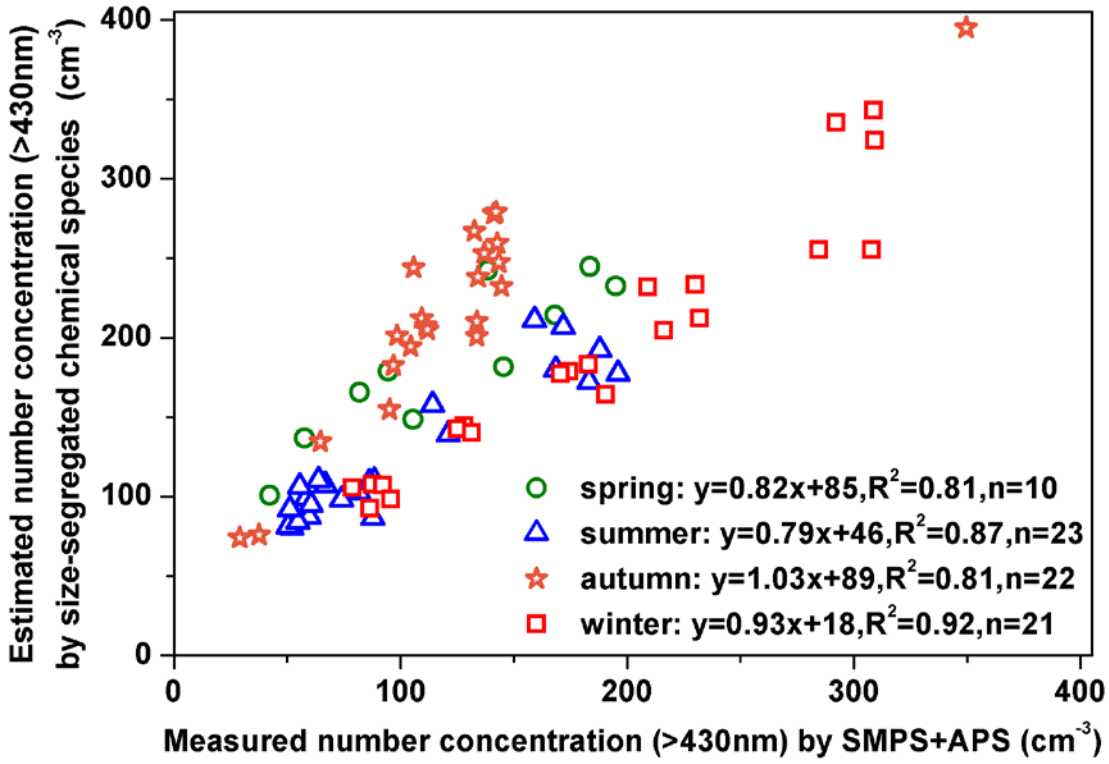

Fig. 5. Correlations between the estimated and SMPS- and APS-measured particle number concentrations (430 nm-10 μm) in four seasons.

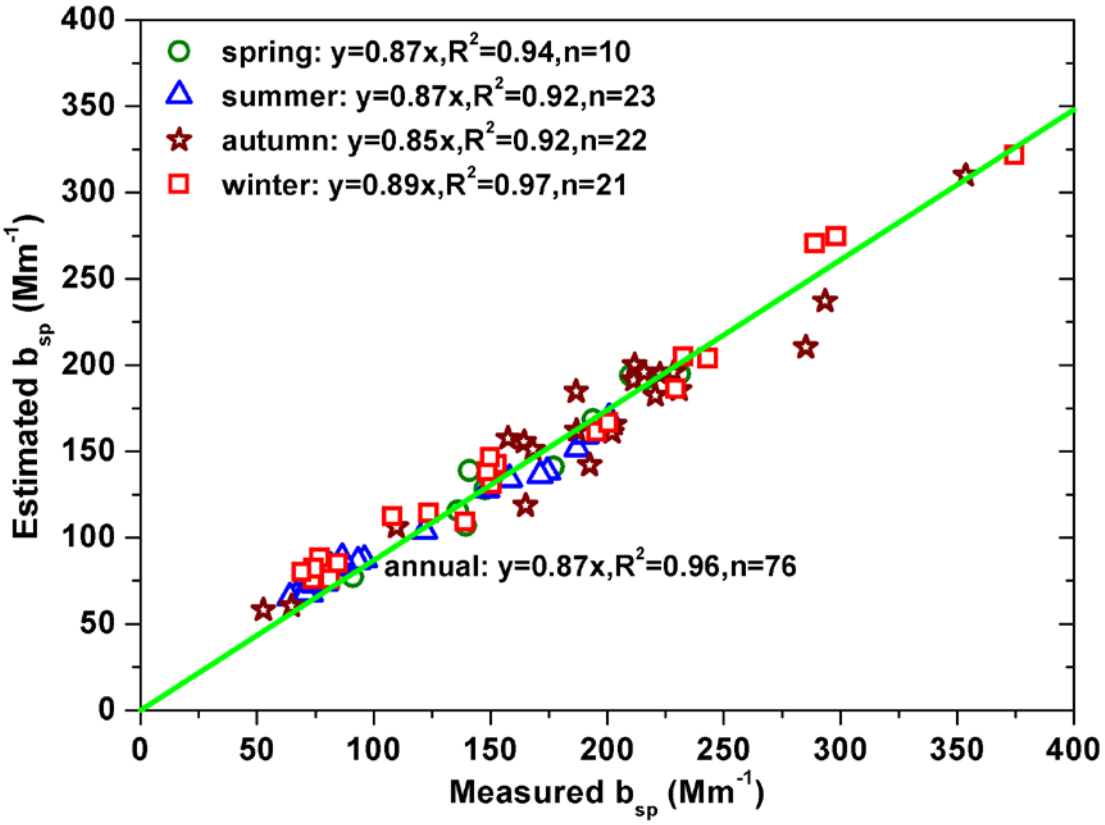

Fig. 6. Correlations between the measured b_{sp} (<100 μm) at wavelength of 520 nm under dry condition (relative humidity <30%) and estimated b_{sp} (<10 μm) at wavelength of 550 nm under dry condition (relative humidity =40%) in four seasons.

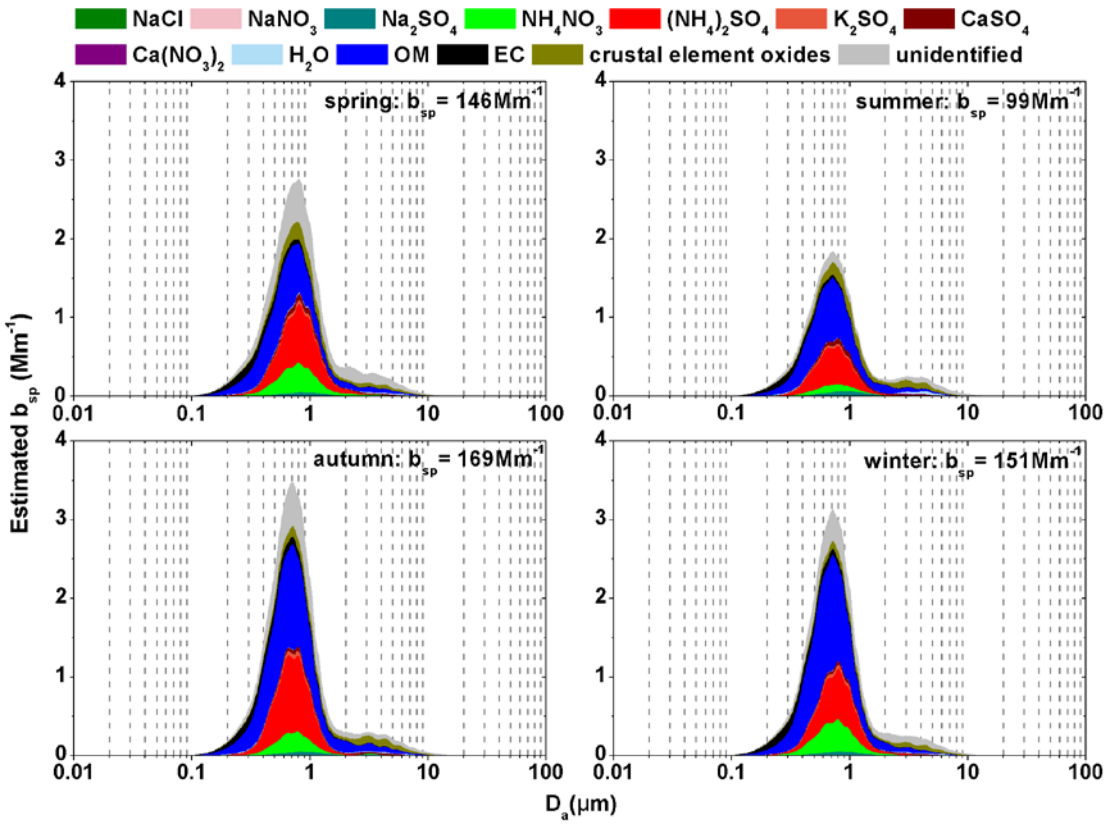

Fig. 7. The contributions of continuous log-normal size distributions of chemical species on the estimated b_{sp} in four seasons ($dlogD_a$=0.01μm).

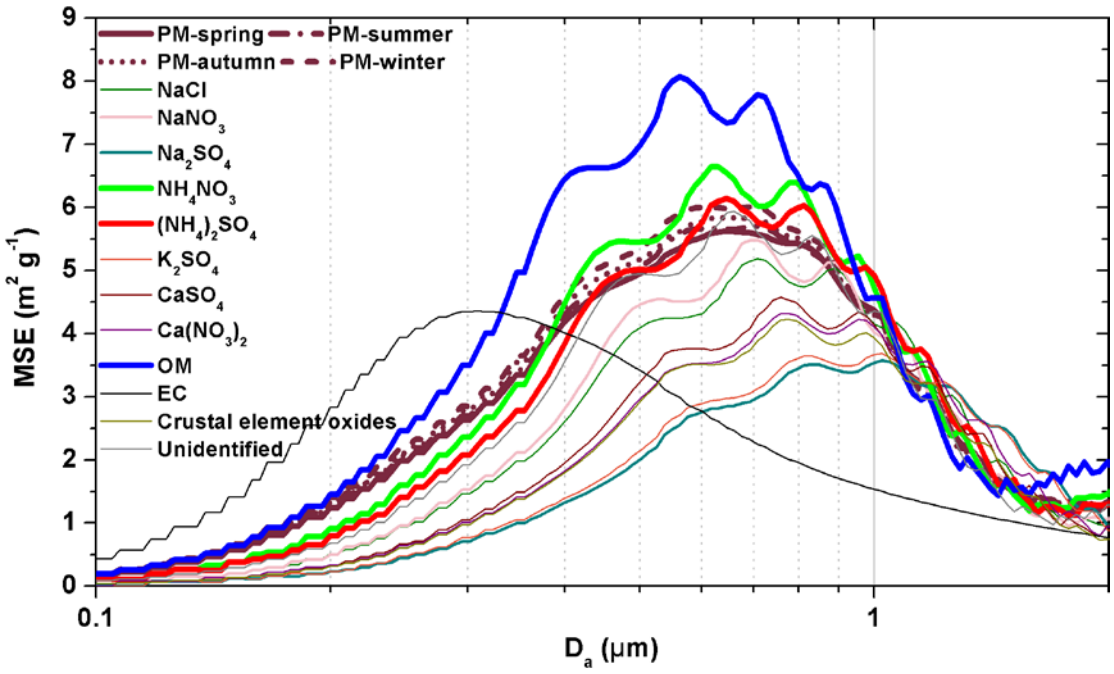

Fig. 8. Continuous log-normal size distributions of fine particle (<2.1μm) mass scattering efficiencies (MSEs) in four seasons and the MSEs of chemical species at wavelength of 550 nm under dry condition (relative humidity =40%) in urban Guangzhou.

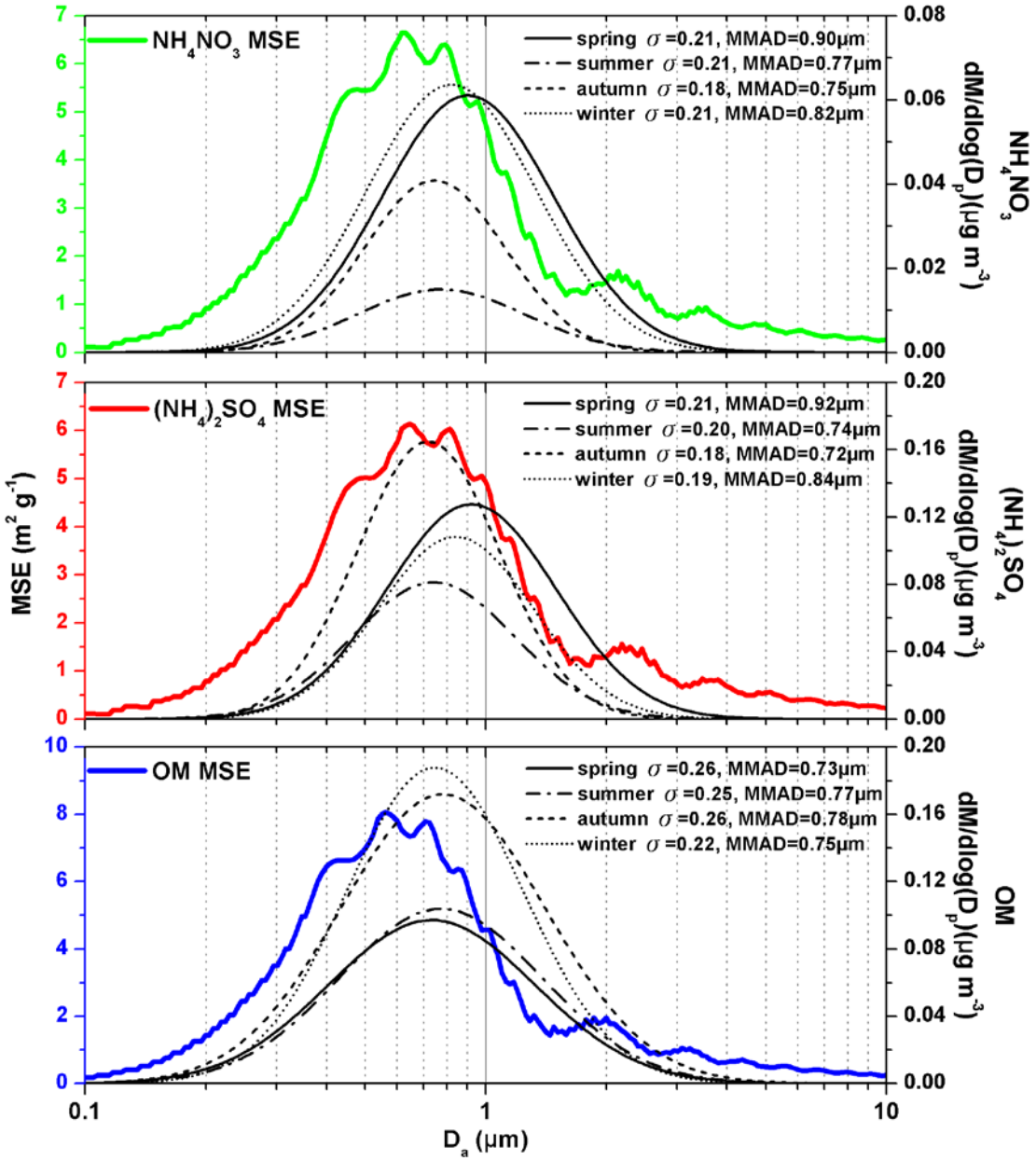

Fig. 9. Continuous log-normal size distributions of $(NH_4)_2SO_4$ (a), NH_4NO_3 (b) and OM (c) mass scattering efficiencies (MSEs), mass concentrations, their σ values and MMADs in the droplet mode at wavelength of 550 nm under dry condition (relative humidity =40%).